Pictorial Representation of Anisotropy and Macroscopic Reorientations of Samples in Solid-State NMR: Second-Order Interactions

C. Bonhomme* and J. Livage

Laboratoire de Chimie de la Matière Condensée, UMR CNRS 7574, Université Pierre et Marie Curie, 4 Place Jussieu, 75252 Paris, Cedex 05, France

Received: July 14, 1998; In Final Form: October 28, 1998

The representation of second-order broadening effects in solid-state NMR by general fourth-degree surfaces is presented. Static second-order quadrupolar and "dipolar−quadrupolar" interactions are treated in a unified way. Most experiments involving the fast reorientation of samples such as magic-angle spinning, variable-angle spinning, dynamic-angle spinning, and double-rotation and multiple-quantum magic-angle spinning are also illustrated by using averaged fourth-degree surfaces. The equations of the surfaces are derived analytically and allow the derivation of most results concerning these experiments. This article is an extension of the representation of the first-order effects by quadrics to more complex broadening effects. Multidimensional experiments will also be discussed in this frame. It can be noted that this approach is essentially Cartesian. $P_2(\cos\theta)$ and $P_4(\cos\theta)$ Legendre polynomials are not explicitly used in this work.

1. Introduction

Anisotropy is a common feature in solid-state NMR in the presence of a strong magnetic field B_o. Indeed, all internal interactions at a given nucleus, such as chemical shift anisotropy (CSA), homo- and heteronuclear dipolar coupling, and quadrupolar interaction (if $I > 1/2$), are characterized by their anisotropy, giving the "strength" of the considered interaction. This leads to broadened patterns (in the frequency domain), such as lines subjected to CSA,[1] Pake doublets[2] (dipolar), first-order quadrupolar satellites,[3] and central transitions broadened by second-order quadrupolar effects.[4] Two more quantities can be defined to fully characterize a given pattern: the asymmetry (η), which governs the "shape" of the line, and the isotropic value of the interaction. This isotropic value is obtained (neglecting solvent effects) in liquid-state NMR. In this case, the average of the interaction is directly measured. All internal interactions can be described by second-rank symmetrical tensors.[5] First-order interactions can be well represented by the so-called "representation ellipsoid". Indeed, the interactions can be described by second-degree polynomials, involving classical trigonometric functions. The intersection of these ellipsoids in the B_o direction gives directly such polynomials. The "representation ellipsoid" is used in the frame of solid-state NMR[6] but more generally in physics.[7] A given tensor is characterized by three principal components and three angles (Euler angles), which orient the considered principal axes system (PAS). In the PAS, the tensor is diagonal. It is well-known that the "representation ellipsoid" implies that the three principal components are strictly positive. When one (or more) principal component is negative (or zero), the "representation ellipsoid" fails. Several authors[8,9] used recently a more complex representation involving ovaloids. We have shown in a previous article[10] that the "representation ellipsoid" could be extended to generalized quadrics (including cylinders, hyperboloids, and planes), accounting for every set of principal components. In this approach, only second-degree surfaces are considered (ovaloids correspond to sixth-order surfaces). When a given interaction is comparable to the Zeeman interaction, second-order effects are predicted and first-order perturbation theory fails. In this case, fourth-degree trigonometric polynomials are involved.[11] It is then obvious that quadrics cannot represent correctly such effects.[10] We shall demonstrate in this article that static second-order shifts of lines can be safely illustrated by general fourth-degree surfaces. The equations of these surfaces in the corresponding PAS are derived analytically.

When several lines are present, the obtained spectrum is generally featureless, accounting for anisotropy of the different interactions. Resolution is therefore usually low for static powders. Nethertheless, it was shown in the late 1950s[12,13] that macroscopic reorientation of samples at a particular angle ($\theta = \zeta_m = 54.74°$) could average first-order interactions, leading to high-resolution spectra. θ corresponds to the macroscopic angle between the rotor axis and B_o. The magic-angle spinning (MAS) technique is now widely used, and very rapid rotation speeds (up to 33 kHz) are attained. We have shown that the effects of MAS and variable-angle spinning (VAS, with $\theta \neq \zeta_m$) on first-order interactions could be graphically interpreted by using averaged quadrics.[10] This representation is very simple, as standard Cartesian transformations (involving 3×3 matrixes) are necessary. The noncontinuous version of MAS (magic-angle hopping or MAH) was illustrated as well.

It is well-known that rapid MAS cannot totally remove second-order broadening effects.[14−16] In the late 1980s, more complicated reorientation schemes of samples were implemented. The dynamic-angle spinning (DAS)[16−19] and double-rotation (DOR)[20,21] of samples allow indeed the total suppression of second-order effects. These techniques were developped especially in the frame of half-integer quadrupolar nuclei (the central transition (−1/2, 1/2) being actually under investigation). Recently, a novel scheme involving multiple-quantum transitions and classical MAS was proposed in the literature and successfully applied to the study of half-integer quadrupolar nuclei.[22,23] This new and appealing technique is now reffered to as multiple-quantum magic-angle spinning (MQ-MAS). The mathematical treatment of DAS, DOR and MQ-MAS is now well established and based on irreducible tensors, Wigner matrixes, and the

10.1021/jp9830171 CCC: $18.00
Published on Web 01/12/1999

ingenious derivation of Hamiltonians in terms of $P_2(\cos\theta)$ and $P_4(\cos\theta)$ (the second- and fourth-degree Legendre polynomials).[16,23] We shall show that averaged fourth-order surfaces are suitable for the direct representation of DAS, DOR, and MQ-MAS. One advantage of this approach is related to its mathematical simplicity; the Cartesian representation of tensors and Cartesian transformations of frames (involving 3×3 matrixes) are the only prerequisites. No explicit reference to Legendre polynomials will be made. The equations of the averaged surfaces will be obtained analytically, and most results concerning the DAS, DOR, and MQ-MAS experiments will be then easily derived.

In this article, the following plan is adopted. Section 2 is devoted to the representation of static second-order effects by fourth-degree surfaces. In this section, the central transition of half-integer quadrupolar nuclei is mainly investigated. Section 3 deals with the representation by surfaces of the dipolar coupling between a $I = 1/2$ spin and a S quadrupolar nucleus. In this case, second-order effects are also involved. Section 4 is devoted to the representation of MAS and VAS on second-order interactions, introducing averaged surfaces. Section 5 is related to the DAS, DAH (dynamic-angle hopping), and DOR experiments. The exact derivation of DAS angle pairs is given. Section 6 is devoted to the MQ-MAS and MQ-VAS (multiple-quantum variable-angle spinning) methodologies. Averaged surfaces allow us to derive the main results of these experiments for $I = n/2$ ($n = 3, 5, 7, 9$).

The "Solve" routine of Mathematica was sometimes used. All 3D representations were done by using graphical routines of Mathematica.

2. Quadrupolar Interaction: Representation of First- and Second-Order Effects in a Static Experiment

In the presence of a strong external magnetic field B_o, the Hamiltonian of a nuclear spin with a quadrupole moment ($I > 1/2$) can be written[6,24]

$$\hat{H} = \hat{H}_Z + \hat{H}_Q \tag{2.1}$$

$\hat{H}_Z$ corresponds to the Zeeman Hamiltonian, whereas $\hat{H}_Q$ corresponds to the quadrupolar Hamiltonian. Moreover, we suppose that $\hat{H}_Q$ can be treated as a perturbation of the Zeeman interaction. Following Harris,[24] the quadrupolar interaction $\hbar^{-1}\hat{H}_Q$ (in angular velocity units) may be represented by a second-rank symmetrical tensor [**q**], such that $\hbar^{-1}\hat{H}_Q = k_Q I[\mathbf{q}]I$. k_Q adjusts the magnitude and dimension of the [**q**] tensor. In the PAS (or XYZ), [**q**] is diagonal and q_{ii} ($i = X, Y,$ and Z) are the principal components. In the respective PAS,

$$k_Q[\mathbf{q}] = \frac{e^2Q}{2I(2I-1)\hbar}\begin{bmatrix} q_{xx} & 0 & 0 \\ 0 & q_{yy} & 0 \\ 0 & 0 & q_{zz} \end{bmatrix} \tag{2.2}$$

Q corresponds to the quadrupole moment of the nucleus and $eq_{ii} = V_{ii}$ are the Cartesian components of the electric field gradient (EFG). This tensor in traceless (in agreement with the Laplace equation, that is, $\sum_{X,Y,Z} q_{ii} = 0$). Therefore, only two independent parameters are required:

$$eq_{ZZ} = V_{ZZ} \tag{2.3a}$$

which is related to the anisotropy of the interaction and

$$\eta_Q = \frac{q_{XX} - q_{YY}}{q_{ZZ}} \qquad (0 \le \eta_Q \le 1) \tag{2.3b}$$

which corresponds to the asymmetry, using the convention

$$|q_{ZZ}| \ge |q_{YY}| \ge |q_{XX}| \tag{2.4}$$

Other conventions may be found in the literature.[25] The [**q**] tensor is not necessarily axially symmetric; that is, η_Q may be different from zero. To estimate the effects of the quadrupolar interaction on the line shapes, the diagonal tensor $[\mathbf{q}]_{PAS}$ must be expressed in the laboratory (LAB) frame ($X_oY_oZ_o$), where the B_o direction and Z_o are coincident. The LAB frame is derived from the quadrupolar PAS frame by the Euler angles ($\alpha_o,\beta_o,\gamma_o$), which are presented in Figure 1. The various energy levels corresponding to eqs 2.1 and 2.2 can be written as $E_m = E_m^{(0)} + E_m^{(1)} + E_m^{(2)}$ ($-I \le m \le I$). The different terms of this expression can be obtained by using standard second-order perturbation theory.[11] Assuming $\eta_Q = 0$,

$$E_m^{(0)} = -\hbar\,\gamma\,B_o\,m \tag{2.5a}$$

$$E_m^{(1)} = \frac{3}{4}\frac{h}{2I(2I-1)}C_Q(3\cos^2\beta_o - 1)\left[m^2 - \frac{1}{3}I(I+1)\right] \tag{2.5b}$$

$$E_m^{(2)} = -hm\left[\frac{3C_Q}{2I(2I-1)}\right]^2\frac{2\pi}{12\gamma B_o}\left\{\frac{3}{2}\cos^2\beta_o(1-\cos^2\beta_o)\times[8m^2 - 4I(I+1) + 1] + \frac{3}{8}(1-\cos^2\beta_o)^2[-2m^2 + 2I(I+1) - 1]\right\} \tag{2.5c}$$

γ is the gyromagnetic ratio of the nucleus of interest and $\gamma B_o = \omega_o$. $C_Q = (e^2qQ)/h$ is the quadrupole coupling constant. The first-order quadrupolar shift corresponding to two consecutive levels ($m - 1$, m) (expressed in angular velocity units) is then derived.

$$\omega_{m-1,m}^{(1),\text{static}} = \hbar^{-1}(E_{m-1}^{(1)} - E_m^{(1)}) = \frac{3(1-2m)}{4I(2I-1)}\frac{e^2Q}{\hbar}\frac{1}{2}q_{ZZ}(3\cos^2\beta_o - 1) \tag{2.6}$$

The expression given by eq 2.6 can be generalized to $\eta_Q \neq 0$.

$$\omega_{m-1,m}^{(1),\text{static}} = \frac{3(1-2m)}{4I(2I-1)}\frac{e^2Q}{\hbar}\frac{1}{2}q_{ZZ}(3\cos^2\beta_o - 1 + \eta_Q\sin^2\beta_o\cos 2\alpha_o) = \frac{3(1-2m)}{4I(2I-1)}\frac{e^2Q}{\hbar}q_{Z_oZ_o} \tag{2.7a}$$

with

$$q_{Z_oZ_o} = \cos^2\alpha_o\sin^2\beta_o\,q_{XX} + \sin^2\alpha_o\sin^2\beta_o\,q_{YY} + \cos^2\beta_o\,q_{ZZ} \tag{2.7b}$$

For $I = n/2$ ($n = 3, 5, 7, 9$), the so-called central transition ($m = 1/2$) is not shifted by the first-order quadrupolar interaction. $m \neq 1/2$ corresponds to the $(2I - 1)$ satellites. Though eqs 2.7a and 2.7b are strictly analogous, eq 2.7b allows us to give a simple pictorial representation of the anisotropy induced by the quadrupolar interaction.[10] As stated above, the tensor [**q**] is traceless. It implies that at least two principal components are

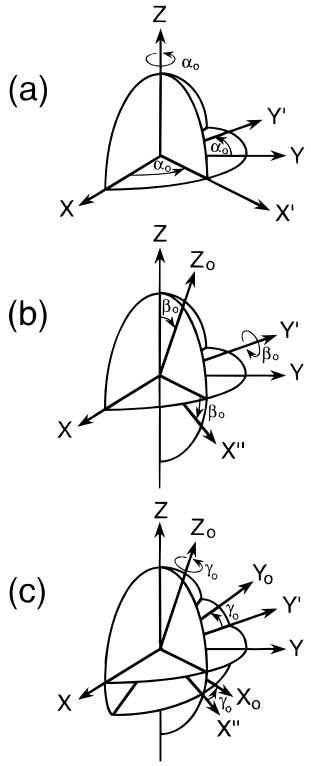

Figure 1. Definitions of the Euler angles (α_o, β_o, γ_o) transforming a given PAS frame (XYZ) into the LAB frame ($X_oY_oZ_o$). (a) PAS frame is rotated counterclockwise around the Z axis by α_o. This rotation generates a new frame ($X'Y'Z$). (b) counterclockwise rotation of the ($X'Y'Z$) frame around Y' by β_o generates a second intermediate frame ($X''Y'Z_o$). (c) This second intermediate frame is rotated counterclockwise by γ_o around Z_o, resulting in the ($X_oY_oZ_o$) LAB frame. Using these definitions, α_o and β_o represent the polar angles of the B_o direction in the PAS.

of opposite signs (they can be eventually zero). As an example, we assume that $q_{XX} > 0$, $q_{YY} > 0$, and $q_{ZZ} < 0$. Let us define the following quadrics (second-degree surfaces) in the quadrupolar PAS.

$$q_{XX}X^2 + q_{YY}Y^2 - |q_{ZZ}|Z^2 = 1 \qquad (2.8a)$$

$$q_{XX}X^2 + q_{YY}Y^2 - |q_{ZZ}|Z^2 = -1 \qquad (2.8b)$$

Equations 2.8a and 2.8b correspond to elliptical hyperboloids of one and two sheets, respectively. They are represented in Figure 2. When B_o is oriented from the quadrupolar PAS by the Euler angles (α_o, β_o, γ_o), it is located in the plane containing the $X'(\alpha_o)$ and Z axes (see Figures 1 and 2). The intersection of the hyperboloid of one sheet (eq 2.8a) by the $X'(\alpha_o)Z$ plane corresponds to an hyperbola, whose equation in $X'(\alpha_o)Z$ is

$$(\cos^2 \alpha_o\, q_{XX} + \sin^2 \alpha_o\, q_{YY})X'^2 - |q_{ZZ}|Z^2 = 1 \qquad (2.9)$$

This hyperbola exhibits two asymptotes, oriented from Z by $\Psi(\alpha_o)$ (Figure 2a). The expression of $\tan^2 \Psi(\alpha_o)$ is given by[10]

$$\tan^2 \Psi(\alpha_o) = \frac{|q_{ZZ}|}{\cos^2 \alpha_o\, q_{XX} + \sin^2 \alpha_o\, q_{YY}} \qquad (2.10)$$

Assuming that $\beta_o > \Psi(\alpha_o)$, the radius r corresponding to the intersection of the hyperbola in the B_o direction is derived using $X' = r \sin \beta_o$, $Z = r \cos \beta_o$, and eq 2.9. One obtains

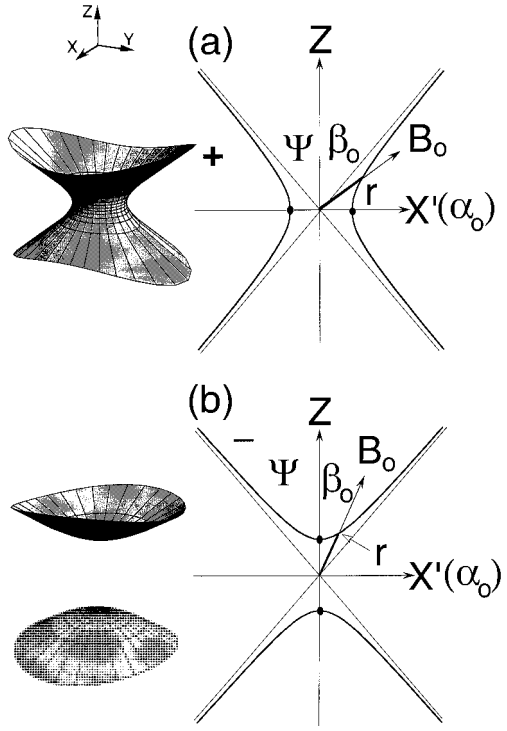

Figure 2. Pictorial representation of anisotropic first-order quadrupolar interaction for $q_{XX} > 0$, $q_{YY} > 0$, and $q_{ZZ} < 0$. Intersections by the plane containing B_o are also given. (a) Elliptical hyperboloid of one sheet. $\tan^2 \Psi(\alpha_o)$ is given by eq 2.10. Intersections with the $X'(\alpha_o)$ axis are given by $\pm(\cos^2 \alpha_o\, q_{XX} + \sin^2 \alpha_o\, q_{YY})^{-1/2}$. When $\beta_o > \Psi(\alpha_o)$, the equation $(+r^{-2}) = q_{z_oz_o}$ holds. The sign of the first member of the equation is emphasized. (b) Elliptical hyperboloid of two sheets. Intersections with the Z axis are given by $\pm|q_{ZZ}|^{-1/2}$. When $\beta_o < \Psi(\alpha_o)$, the equation $(-r^{-2}) = q_{z_oz_o}$ holds. The sign of the first member of the equation is emphasized.

$$r = (\cos^2 \alpha_o \sin^2 \beta_o\, q_{XX} + \sin^2 \alpha_o \sin^2 \beta_o\, q_{YY} - \cos^2 \beta_o\, |q_{ZZ}|)^{-1/2} \qquad (2.11)$$

When eqs 2.11 and 2.7b are compared, it follows that $(+r^{-2}) = q_{Z_oZ_o}$. The sign + is emphasized in this expression as well as in Figure 2a. Therefore, a simple pictorial representation of $q_{Z_oZ_o}$ is given. When $\beta_o \rightarrow \Psi(\alpha_o)$, $q_{Z_oZ_o} \rightarrow 0$, as $r \rightarrow \infty$. The zero value of the tensor component $q_{Z_oZ_o}$ is attained, but in this case, it does not correspond to a principal component. When $\beta_o < \Psi(\alpha_o)$, the B_o direction does not intersect the hyperbola presented in Figure 2a. However, one can use the complementary quadric given by eq 2.8b (Figure 2b). Again, the intersection of this quadric by the $X'(\alpha_o)Z$ plane corresponds to an hyperbola, whose equation in $X'(\alpha_o)Z$ is

$$-(\cos^2 \alpha_o\, q_{XX} + \sin^2 \alpha_o\, q_{YY})X'^2 + |q_{ZZ}|Z^2 = +1 \qquad (2.12)$$

Using eq 2.12 and assuming that $\beta_o < \Psi(\alpha_o)$, the intersection radius r is then given by

$$r = [-(\cos^2 \alpha_o \sin^2 \beta_o\, q_{XX} + \sin^2 \alpha_o \sin^2 \beta_o\, q_{YY}) + \cos^2 \beta_o\, |q_{ZZ}|]^{-1/2} \qquad (2.13)$$

It follows that $(-r^{-2}) = q_{Z_oZ_o}$. Again, the sign − is emphasized in this expression as well as in Figure 2b. When $\beta_o = 0$, $(-r^{-2}) = -|q_{ZZ}| = q_{ZZ}$ and the negative principal component is attained. It has thus been shown that first-order effects of the quadrupolar interaction can be represented by two complementary quadrics. It is interesting to note that in this case, the popular "representa-

tion ellipsoid"[6] fails, as some principal components are negative. When $\eta_Q = 0$, the surfaces are of revolution, with Z as the unique axis of revolution. Moreover, when one principal component is zero, a pictorial representation of anisotropy is then given by a set of two complementary hyperbolical cylinders.[10] The important point is that second-degree surfaces (that is quadrics) are suitable for the representation of first-order effects. We have also shown previously that they are also suitable for the direct representation of macroscopic reorientation of samples and that they account for the suppression of first-order interactions under MAS (assuming that the rotation speed of the sample is much higher than the involved interactions).

We now turn to quadrupolar second-order effects. The quadrupolar interaction can be very large, so that the first-order perturbation theory is not always adequate. When $\hat{H}_Q$ becomes comparable to $\hat{H}_Z$ (see eq 2.1), second-order effects must be taken into account. For $I = n/2$ ($n = 3, 5, 7, 9$), the central transition ($-1/2, 1/2$) is mainly observed, with the satellites lines being smeared out over the megahertz range. In the following sections, the central transition will be mainly considered (except in Section 6). Using eq 2.5c and assuming $\eta_Q = 0$, the second-order quadrupolar shift of the central line is given by

$$\omega^{(2),\mathrm{static}}_{-1/2,1/2} = \hbar^{-1}(E^{(2)}_{-1/2} - E^{(2)}_{1/2}) = C_{-1/2,1/2}\left[\frac{3}{8}\sin^2\beta_o(9\cos^2\beta_o - 1)\right] \quad (2.14)$$

(omitting ω_{cs} corresponding to the true chemical shift). The constant $C_{-1/2,1/2}$ is related to the quadrupole coupling constant C_Q and is inversely proportional to ω_o as

$$C_{-1/2,1/2} = -\frac{4\pi^2}{6\omega_o}\left[\frac{3C_Q}{2I(2I-1)}\right]^2[(I(I+1) - 3/4] \quad (2.15)$$

It is interesting to note that the anisotropy of the central transition due to second-order effects is represented by the polynomial $Q(\beta_o) = 3/8 \sin^2\beta_o (9\cos^2\beta_o - 1)$; β_o orient B_o from the quadrupolar PAS (Figure 1). Equation 2.14 can be generalized for $\eta_Q \neq 0$ as[25]

$$\omega^{(2),\mathrm{static}}_{-1/2,1/2} = C_{-1/2,1/2}[A(\alpha_o, \eta_Q)\cos^4\beta_o + B(\alpha_o, \eta_Q)\cos^2\beta_o + C(\alpha_o, \eta_Q)] \quad (2.16)$$

with

$$A(\alpha_o,\eta_Q) = -27/8 + (9/4)\eta_Q\cos 2\alpha_o - (3/8)(\eta_Q\cos 2\alpha_o)^2 \quad (2.17a)$$

$$B(\alpha_o,\eta_Q) = 30/8 - (1/2)\eta_Q^2 - 2\eta_Q\cos 2\alpha_o + (3/4)(\eta_Q\cos 2\alpha_o)^2 \quad (2.17b)$$

$$C(\alpha_o,\eta_Q) = -3/8 + (1/3)\eta_Q^2 - (1/4)\eta_Q\cos 2\alpha_o - (3/8)(\eta_Q\cos 2\alpha_o)^2 \quad (2.17c)$$

$C_{-1/2,1/2}$ is given in eq 2.15. Again, the anisotropy is represented by the polynomial $R(\alpha_o,\beta_o) = A(\alpha_o,\eta_Q)\cos^4\beta_o + B(\alpha_o,\eta_Q)\cos^2\beta_o + C(\alpha_o,\eta_Q)$. To give a suitable pictorial representation of the second-order effects on the central transition, one must connect a surface (or a set of complementary surfaces) with the polynomials $Q(\alpha_o)$ and $R(\alpha_o,\beta_o)$. $Q(\alpha_o)$ and $R(\alpha_o,\beta_o)$ are obviously fourth-degree polynomials of the trigonometric functions. It is then evident that second-degree surfaces such as quadrics cannot be connected to $Q(\alpha_o)$ and $R(\alpha_o,\beta_o)$. Indeed, they allow only a satisfactory representation of second-degree polynomials (see eqs 2.7b and 2.11). Novel surfaces must be considered. The equations of these surfaces in the quadrupolar PAS will be first derived for $\eta_Q = 0$ and then generalized for $\eta_Q \neq 0$. In the PAS, the relations $X = r\cos\alpha_o\sin\beta_o$, $Y = r\sin\alpha_o\sin\beta_o$, and $Z = r\cos\beta_o$ hold. It follows that $X^2 + Y^2 = r^2\sin^2\beta_o$ and $Z^2 = r^2\cos^2\beta_o$. The polynomial $Q(\alpha_o)$ can be written $Q(\alpha_o) = (3/8)\sin^2\beta_o(8\cos^2\beta_o - \sin^2\beta_o)$ or

$$r^4Q(\beta_o) = (3/8)(r^2\sin^2\beta_o)[8(r^2\cos^2\beta_o) - (r^2\sin^2\beta_o)] = (3/8)(X^2 + Y^2)[8Z^2 - (X^2 + Y^2)] \quad (2.18)$$

Now, we consider the fourth-degree surface, whose equation in the PAS is

$$(3/8)(X^2 + Y^2)[8Z^2 - (X^2 + Y^2)] = 1 \quad (2.19)$$

This surface is obviously of revolution, with the Z axis as the axis of revolution. It is presented in Figure 3a, as well as the intersection of this surface by any plane containing the Z axis (Figure 3b). The intersection curve exhibits two asymptotes, oriented from the Z axis by $\Phi = 0°$ and Φ_o (see Figure 3b). Φ_o is characterized by $\tan^2\Phi_o = 8$ or $\Phi_o = 70.53°$. The minimum radius r_{min} is obtained for χ_o. The exact value of χ_o is obtained by derivation of the expression $\sin^2\beta_o(8\cos^2\beta_o - \sin^2\beta_o)$. It follows that $\chi_o = (1/2)\arccos(1/9)$ or $\chi_o = 41.81°$ and $r_{min} = (2/3)^{-1/4}$. Using eq 2.19, the radius r corresponding to the intersection of the surface in the B_o direction (characterized by the polar angles (α_o,β_o)) is then derived as

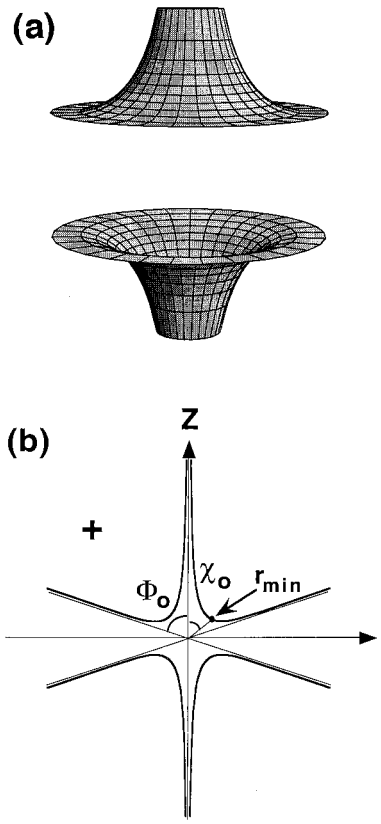

Figure 3. (a) Fourth-degree surface corresponding to eq 2.19 ($\eta_Q = 0$). The Z axis of the PAS corresponds to the axis of revolution. (b) Section of the surface by any plane containing the Z axis. The asymptotes are given by $\Phi = 0°$ and $\Phi_o = 70.53°$ (see text). $r_{min} = (2/3)^{-1/4}$ is associated to the angle $\chi_o = 41.81°$. The sign + is emphasized.

$$r = [(3/8)\sin^2\beta_o(8\cos^2\beta_o - \sin^2\beta_o)]^{-1/4} \quad (2.20a)$$

$$(+r^{-4}) = Q(\beta_o) \quad (2.20b)$$

Equation 2.20b gives therefore a simple pictorial interpretation of the second-order interaction described by $Q(\beta_o)$; the intersection of the surface presented in Figure 3 in the B_o direction is directly related to the second-order quadrupolar shift. The sign + is emphasized in eq 2.20b as well as in Figure 3. When $\beta_o \rightarrow 0°$ or Φ_o, $r \rightarrow \infty$ and $Q(\beta_o) \rightarrow 0$; the second-order quadrupolar shift vanishes. When $\beta_o = \chi_o$, the shift is maximum (in absolute value), as r is minimum. Obviously, when $\beta_o > \Phi_o$, no intersection is obtained. One can then use the complementary fourth-degree surface, whose equation in the PAS is given by

$$(3/8)(X^2 + Y^2)[8Z^2 - (X^2 + Y^2)] = -1 \quad (2.21)$$

Again, this surface is of revolution and is presented in Figure 4a. The radius r corresponding to the intersection of the surface in the B_o direction is given by

$$r = [-(3/8)\sin^2\beta_o(8\cos^2\beta_o - \sin^2\beta_o)]^{-1/4} \quad (2.22a)$$

$$(-r^{-4}) = Q(\beta_o) \quad (2.22b)$$

The sign − is emphasized in this equation and in Figure 4. The relation between r and $Q(\beta_o)$ is now different but remains easy to visualize. Therefore, the second-order quadrupolar interaction for the central transition is fully represented by a set of two complementary fourth-degree surfaces. This situation is rather similar to that encountered for first-order effects (see above); indeed, a set of two hyperboloids was necessary for the complete pictorial description of anisotropy. However, in the case of second-order effects, two major differences are noted: (i) the involved surfaces are fourth-degree surfaces and (ii) $(\pm r^{-4})$ is related to the anisotropic shift instead of $(\pm r^{-2})$. Finally, it is possible to relate the powder pattern of the central transition[4]

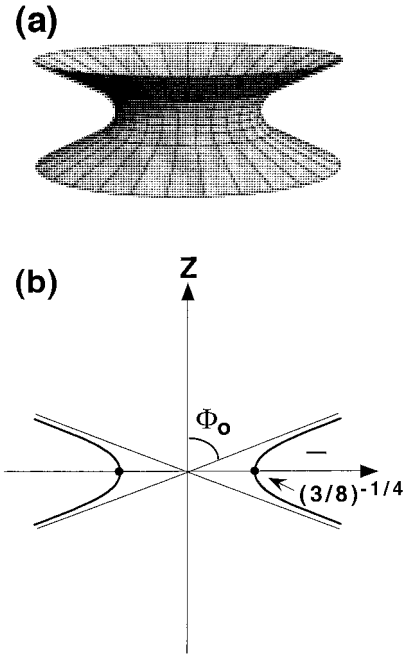

Figure 4. (a) Fourth-degree surface corresponding to eq 2.21 ($\eta_Q = 0$). The Z axis of the PAS corresponds to the axis of revolution. (b) Section of the surface by any plane containing the Z axis. The asymptote is given by $\Phi_o = 70.53°$. The sign − is emphasized.

in a static experiment and the particular angles Φ_o and χ_o presented above (Figure 5).

When $\eta_Q \neq 0$, the anisotropy related to the central transition is given by the polynomial $R(\alpha_o,\beta_o)$ (see eq 2.16). We consider the set of two complementary fourth-degree surfaces given in the quadrupolar PAS by

$$aX^4 + bY^4 + cZ^4 + dX^2Y^2 + eX^2Z^2 + fY^2Z^2 = \pm 1 \quad (2.23)$$

where $a-f$ are unknown functions of η_Q for the moment. In the PAS, the following relations hold: $X^4 = r^4\cos^4\alpha_o(1 - \cos^2\beta_o)^2$; $Y^4 = r^4(1 - \cos^2\alpha_o)^2(1 - \cos^2\beta_o)^2$; $Z^4 = r^4\cos^4\beta_o$; $X^2Y^2 = r^4\cos^2\alpha_o(1 - \cos^2\alpha_o)(1 - \cos^2\beta_o)^2$; $X^2Z^2 = r^4\cos^2\alpha_o\cos^2\beta_o(1 - \cos^2\beta_o)$; and $Y^2Z^2 = r^4(1 - \cos^2\alpha_o)\cos^2\beta_o(1 - \cos^2\beta_o)$. Inserting these relations in eq 2.23, we impose moreover that $(\pm r^{-4}) = R(\alpha_o,\beta_o)$. After rewriting $R(\alpha_o,\beta_o)$ in terms of cosine functions, the equation $(\pm r^{-4}) = R(\alpha_o,\beta_o)$ leads to the following system of six linear equations:

$$b = -3/8 + (1/4)\eta_Q - (1/24)\eta_Q^2$$

$$-2b + d = -(1/2)\eta_Q + (3/2)\eta_Q^2$$

$$a + b - d = -(3/2)\eta_Q^2$$

$$4b - 2d + e - f = -(4\eta_Q + 3\eta_Q^2)$$

$$-2b + f = 15/4 + 2\eta_Q + (1/4)\eta_Q^2$$

$$b + c - f = -27/8 - (9/4)\eta_Q - (3/8)\eta_Q^2 \quad (2.24)$$

This system is easily solved, and the complementary fourth-degree surfaces are then given by eq 2.23 and

$$a = -(3/8 + (1/4)\eta_Q + (1/24)\eta_Q^2)$$

$$b = -3/8 + (1/4)\eta_Q - (1/24)\eta_Q^2$$

$$c = -(1/6)\eta_Q^2$$

$$d = -6/8 + (17/12)\eta_Q^2$$

$$e = 3 - (5/2)\eta_Q + (1/6)\eta_Q^2$$

$$f = 3 + (5/2)\eta_Q + (1/6)\eta_Q^2 \quad (2.25)$$

Generally, these surfaces are not of revolution. Sections of these surfaces by the XZ and YZ planes are given in Figures 6 and 7. When $\eta_Q = 0$, eqs 2.19, 2.21, and 2.23 are identical. As a conclusion, we have shown that a direct pictorial representation of second-order effects on the central transition can be proposed, using a set of two complementary fourth-degree surfaces. The analytical expressions of their equations in the PAS have been given. To our knowledge, such a direct Cartesian representation of second-order interactions was never proposed in the literature. It will be seen below that these surfaces are suitable not only for the direct representation of anisotropy but also for a pictorial representation of MAS, VAS, and higher-order trajectories. Before considering the effects of macroscopic sample reorienta-

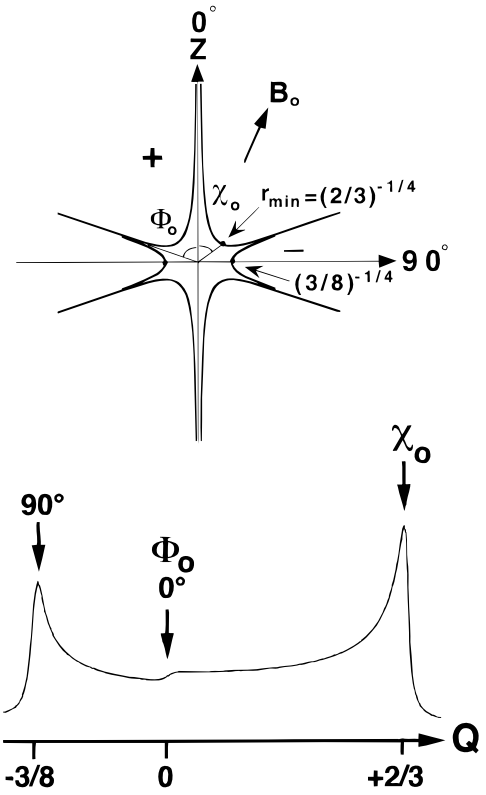

Figure 5. Pictorial representation of second-order interaction using the set of complementary fourth-degree surfaces (eqs 2.19 and 2.21). The signs + and − are emphasized. For particular orientations of B_o in the quadrupolar PAS ($\beta_o = 0°$, χ_o, Φ_o and 90°), the corresponding resonance shifts are indicated on a typical second-order broadened line shape ($\eta_Q = 0$). The quadrupolar dimension is given in $C_{-1/2,1/2}$ units (see eq 2.15).

tions, we illustrate with geometrical surfaces the dipolar coupling of a $I = 1/2$ spin to a quadrupolar S spin (Section 3).

3. Pictorial Representation of Coupled Interactions: Dipolar Coupling to $S > 1/2$

As stated above, higher interactions involve fourth-degree expressions of the basic trigonometric functions. Among them, the dipolar coupling of a I nucleus ($I = 1/2$) to a quadrupolar nucleus S ($S > 1/2$) has been carefully analyzed in the past years, theoretically and experimentally.[26−28] These spin pair systems were especially studied under MAS conditions, leading to "dipolar-coupled" spectra for the I spin. Moreover, it was observed that this residual interaction cannot be completely eliminated by rapid MAS (for the description of rapid MAS on this particular interaction, see Section 4). Originally, asymmetric doublets were observed in spectra related to $^{13}C-^{14}N$ ($S = 1$) pairs.[29] The ^{13}C resonance frequencies associated to the different m_s states of the ^{14}N nucleus were calculated,[26] leading to the following expressions of $\omega_{m_S}^{\text{static}}$:

$$\omega_0^{\text{static}} = \frac{9}{2}\left(\frac{2\pi D C_Q}{Z_N}\right)\cos^2\beta_o(1-\cos^2\beta_o) \qquad (3.1a)$$

$$\omega_{+1}^{\text{static}} = -\omega_0^{\text{static}}/2 + 2\pi D(3\cos^2\beta_o - 1) \qquad (3.1b)$$

$$\omega_{-1}^{\text{static}} = -\omega_0^{\text{static}}/2 - 2\pi D(3\cos^2\beta_o - 1) \qquad (3.1c)$$

where $C_Q = (e^2 q_{ZZ} Q)/h$ is the quadrupole coupling constant, $D = (\mu_o/4\pi)(\hbar/2\pi)(\gamma_C\gamma_N)/r^3_{CN}$ is the dipolar coupling constant,

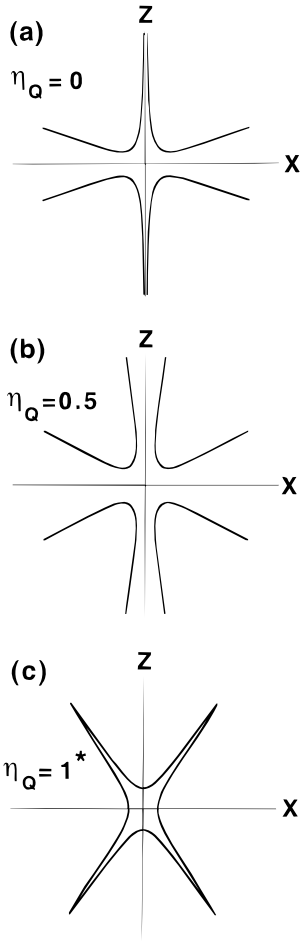

Figure 6. Sections in the XZ plane of the fourth-degree surfaces defined by eq 2.23 for variable η_Q. (XYZ) is the quadrupolar PAS. The corresponding equation is $aX^4 + cZ^4 + eX^2Z^2 = +1$ (see eqs 2.25). (a) $\eta_Q = 0$. Asymptotes are located (from Z) at $\Phi = 0°$ and $\Phi = 70.53°$ ($\cos^2\Phi = 1/9$) (see also Figure 3b). (b) $\eta_Q = 0.5$. Asymptotes are located (from Z) at $\Phi = 8.69°$ ($\cos^2\Phi = (9 + 4\sqrt{2})/15$) and $\Phi = 61.83°$ ($\cos^2\Phi = (9 - 4\sqrt{2})/15$). (c) $\eta_Q = 1$. The asymptote is located (from Z) at $\Phi = 35.26°$ ($\cos^2\Phi = 2/3$). *The curve associated to $aX^4 + cZ^4 + eX^2Z^2 = +1$ is imaginary ($a = -2/3$; $c = -1/6$; $e = 2/3$). $aX^4 + cZ^4 + eX^2Z^2 = -1$ is represented.

and $Z_N = (\gamma_N B_o)/2\pi$ is the Zeeman frequency of the ^{14}N. Equations 3.1 correspond to a special case where $\eta_Q = 0$ and the dipolar and quadrupolar PAS are coincident (the internuclear radius r_{CN} is collinear with the Z axis of the quadrupolar PAS). General expressions are given in ref 26. Obviously, no second-degree surface can give an accurate representation of the shifts represented by eqs 3.1. Following the approach presented in Section 2, we consider the set of general complementary fourth-degree surfaces given in the unique PAS by

$$a_{m_s}(X^2 + Y^2)^2 + b_{m_s}Z^4 + c_{m_s}Z^2(X^2 + Y^2) = \pm 1 \qquad (3.2)$$

These surfaces are of revolution (with Z as the axis of revolution), as only one Euler angle (β_o) is involved in eq 3.1. Moreover, we impose that $(\pm r^{-4}) = \omega_{m_S}^{\text{static}}$ for $m_s = 0$, $+1$, and -1, respectively. Systems of linear equations (comparable to eqs 2.24) are obtained in each case. The obtained a_{m_S}, b_{m_S}, c_{m_S} values are given in Table 1. The corresponding surfaces are presented in Figure 8. One notes that the equation $C_oZ^2(X^2 + Y^2) = -1$ corresponds to an imaginary surface. The surface related to $C_oZ^2(X^2 + Y^2) = +1$ exhibits two asymptotes at 0° and 90°. The shape of this surface is comparable to the one

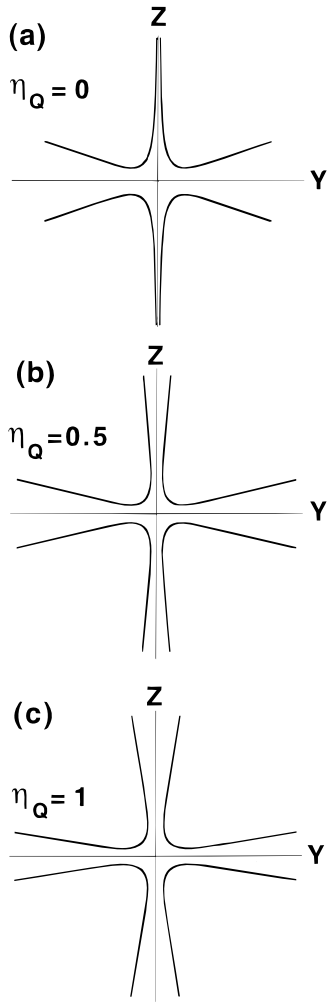

Figure 7. Sections in the *YZ* plane of the fourth-degree surfaces defined by eq 2.23 for variable η_Q. (*XYZ*) is the quadrupolar PAS. The corresponding equation is $bY^4 + cZ^4 + fY^2Z^2 = +1$ (see eq 2.25). (a) $\eta_Q = 0$. The curve is similar to the one presented in Figure 6a. The corresponding surface is of revolution. (b) $\eta_Q = 0.5$. Asymptotes are located (from *Z*) at $\Phi = 5.63°$ ($\cos^2 \Phi = (11 + 4\sqrt{6})/21$) and $\Phi = 76.16°$ ($\cos^2 \Phi = (11 - 4\sqrt{6})/21$)). (c) $\eta_Q = 1$. The asymptotes are located (from Z) at $\Phi = 9.74°$ ($\cos^2 \Phi = (3 + 2\sqrt{2})/6$) and $\Phi = 80.26°$ ($\cos^2 \Phi = (3 - 2\sqrt{2})/6$).

TABLE 1: Values of the Coefficients a_{m_S}, b_{m_S}, c_{m_S} Involved in the Pictorial Representation of the Dipolar Coupling of a $I = 1/2$ Spin Coupled to a Quadrupolar S Spin[a]

	a	*b*	*c*
0	0	0	$(9/2)\ (2\pi D C_Q)/Z_N$
1	$-2\pi D$	$4\pi D$	$2\pi D(1 - 9/4(C_Q/Z_N))$
-1	$+2\pi D$	$-4\pi D$	$-2\pi D(1 + 9/4(C_Q/Z_N))$

[a] C_Q corresponds to the quadrupole coupling constant. *D* is the dipolar constant. Z_N is the Zeeman frequency of the quadrupolar nucleus (see Section 3).

related to the (−1/2,1/2) central transition broadened by second-order effects (see Section 2 and Figure 3). Surfaces related to $m_s = \pm 1$ (parts b and c of Figure 8) include a "classical" dipolar term, corresponding to the expression $\pm 2\pi D(3 \cos^2 \beta_o - 1)$ in eqs 3.1.

4. Rotation of Samples around One Single Axis: MAS and VAS

Andrew and Lowe[12,13] demonstrated first that rapid rotation of samples around the "magic-angle" ($\theta = \zeta_m$) allows the total

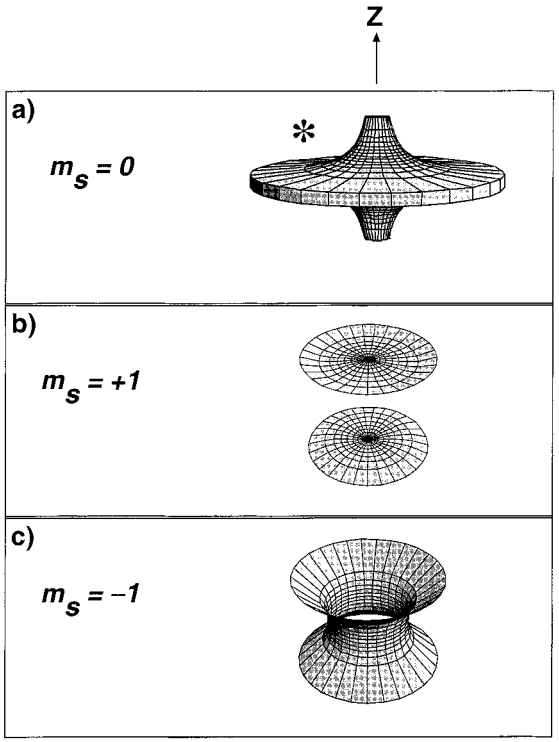

Figure 8. Surfaces of revolution illustrating the dipolar coupling of a *I* spin to a $S > 1/2$ spin (in the quadrupolar PAS). They correspond to $a_{m_S}(X^2 + Y^2)^2 + b_{m_S}Z^4 + c_{m_S}Z^2\ (X^2 + Y^2) = +1$ (see Table 1 and eq 3.2) ($c_o = 1$ and $2\pi D = 10$, in arb. units): (a) $m_s = 0$; (b) $m_s = +1$; (c) $m_s = -1$. *The surface corresponding to $c_o\ Z^2\ (X^2 + Y^2) = -1$ is imaginary ($a_o = b_o = 0$).

suppression of first-order interactions. θ corresponds to the angle between the rotor axis and B_o. When $\theta \neq \zeta_m$, the reorientation technique is known as VAS. Application of MAS and VAS to quadrupolar nuclei was mainly investigated in the early 1980s.[30,31] It was soon demonstrated that MAS cannot completely eliminate the second-order effects on the central transition. In fact, a residual broadening of the line is observed for every θ. We shall now illustrate the effects of MAS and VAS by considering the fourth-degree surfaces presented in Section 2 and simple Cartesian transformations. Most of the results will be demonstrated for $\eta_Q = 0$, using eqs 2.19 and 2.21. They can be extended as well to $\eta_Q \neq 0$ by using eqs 2.23 and 2.25. Finally, it should be noted that this approach is strictly analogous to that used for the direct representation of MAS effects on first-order interactions.[10] Let us consider the central transition of a quadrupolar nucleus, broadened by second-order effects ($\eta_Q = 0$). In the PAS, the pertinent fourth-degree surfaces giving the second-order quadrupolar shift (in $C_{-1/2,1/2}$ units; see eq 2.15) for every crystallite's orientation are

$$(3/8)(X^2 + Y^2)[8Z^2 - (X^2 + Y^2)] = \pm 1 \qquad (4.1)$$

We consider a rotor frame ($X_R Y_R Z_R$), which is oriented by the Euler angles (α, β, γ) from the PAS (Figure 9). Equations 4.1 can be written in ($X_R Y_R Z_R$) by using the matrix **P** and the expressions for X^4, Y^4, ... Y^2Z^2 in terms of X_R, Y_R, and Z_R (see the Appendix). Spinning the sample implies that γ becomes a function of ω_{rot} where $\omega_{rot} = 2\pi\nu_{rot}$ corresponds to the pulsation of the rotor. We suppose that $\nu_{rot} = \infty$, that is, ν_{rot} is much higher than the considered interactions in hertz. When the expressions of X^4, Y^4, ...Y^2Z^2 are expanded (see the Appendix), trigonometric terms involving γ are averaged by considering the following integrals:

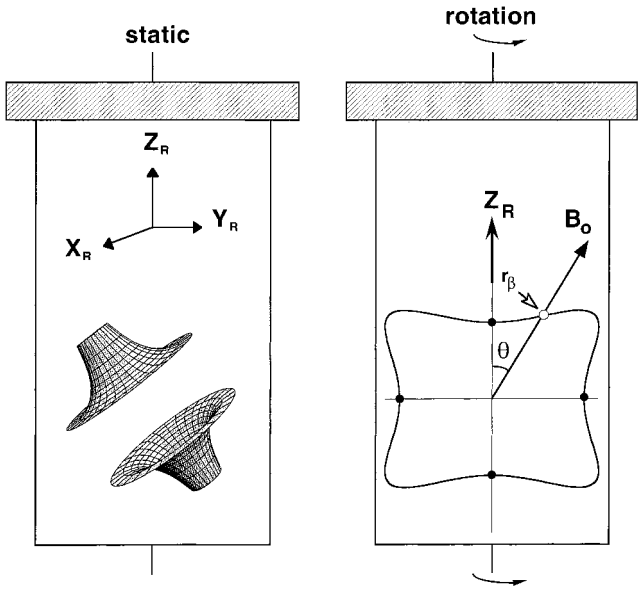

Figure 9. Pictorial representation of rapid rotation of the sample around one axis ($\theta = \zeta_m$, MAS; $\theta \neq \zeta_m$, VAS). In the static rotor (left side), the crystallites are randomly oriented from ($X_R Y_R Z_R$). The surface is drawn in the PAS of each crystallite (characterized by Z, $\eta_Q = 0$). In the rapidly rotating rotor (right side), the corresponding averaged surface is represented. It is of revolution and admits Z_R as the unique axis of revolution. Intersections with the horizontal axis and Z_R are given by $\pm[A(\boldsymbol{\beta})]^{-1/4}$ and $\pm[B(\boldsymbol{\beta})]^{-1/4}$ (see eqs 4.4), respectively (we suppose here that $A(\boldsymbol{\beta}) > 0$ and $B(\boldsymbol{\beta}) > 0$). The intersection of the averaged surface in the B_o direction gives r_β.

$$I_{r,s} = \frac{1}{2\pi}\int_0^{2\pi} (\cos\gamma)^r (\sin\gamma)^s \, d\gamma \qquad (4.2)$$

for $r = 0-4$ and $s = 0-4$ with $(r, s) \neq (0,0)$ and $r + s \leq 4$. Useful values of $I_{r,s}$ are given in Table 2. Under rapid rotation, the averaged fourth-degree surfaces (Figure 9) are given in ($X_R Y_R Z_R$) by

$$A(\boldsymbol{\beta})(X_R^2 + Y_R^2)^2 + B(\boldsymbol{\beta})Z_R^4 + C(\boldsymbol{\beta})Z_R^2(X_R^2 + Y_R^2) = \pm 1 \qquad (4.3)$$

with

$$A(\boldsymbol{\beta}) = (3/64)(-27\cos^4\beta + 14\cos^2\beta + 5)$$

$$B(\boldsymbol{\beta}) = (1/8)(-27\cos^4\beta + 30\cos^2\beta - 3)$$

$$C(\boldsymbol{\beta}) = (3/8)(27\cos^4\beta - 22\cos^2\beta + 3) \qquad (4.4)$$

The averaged surfaces are of revolution with Z_R as the axis of revolution. All these surfaces are different as their equations depend explicitly on β. Moreover, depending on the sign of $A(\boldsymbol{\beta})$, $B(\boldsymbol{\beta})$, and $C(\boldsymbol{\beta})$ (eqs 4.4), variable curves related to eqs 4.3 are obtained. Several of them are presented in Figure 10. In most cases, eqs 4.3 correspond to complementary surfaces. When $A(\boldsymbol{\beta})$, $B(\boldsymbol{\beta})$, and $C(\boldsymbol{\beta})$ are strictly positive, it is evident

TABLE 2: Useful Values of the Integrals $I_{r,s}$ for $(r + s) \leq 4$ and $(r, s) \neq (0, 0)$ (see Section 4 and Eq 4.2)

	s				
r	0	1	2	3	4
0		0	1/2	0	3/8
1	0	0	0	0	
2	1/2	0	1/8		
3	0	0			
4	3/8				

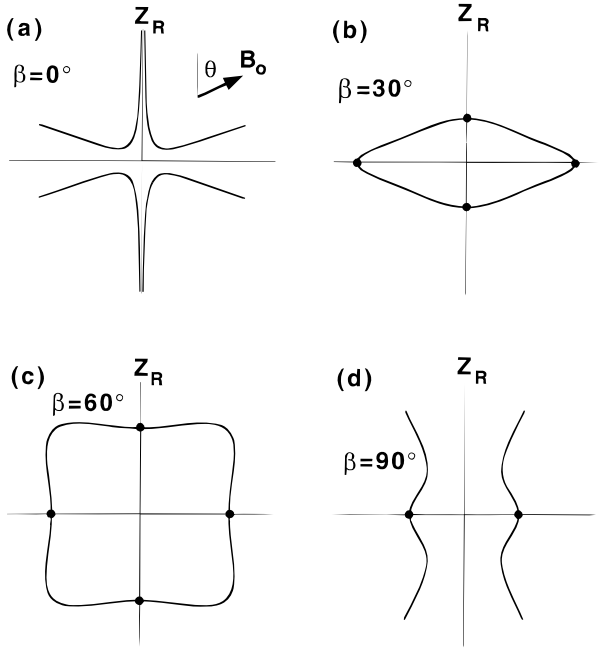

Figure 10. Averaged surfaces of revolution under rapid rotation of the sample. Z_R corresponds to the axis of revolution. B_o is oriented from Z_R by θ. (a) $\beta = 0°$. The curve is comparable to the one presented in Figure 3b. Asymptotes are at 0° and 70.53° (from Z_R). (b) $\beta = 30°$. Intersections with the axes are given by $\pm[A(30°)]^{-1/4}$ and $\pm[B(30°)]^{-1/4}$ (see eqs 4.4). (c) $\beta = 60°$. Intersections with the axes are given by $\pm[A(60°)]^{-1/4}$ and $\pm[B(60°)]^{-1/4}$ (see eqs 4.4). (d) $\beta = 90°$. Intersection with the horizontal axis is given by $\pm[A(90°)]^{-1/4} = \pm(15/64)^{-1/4}$. The asymptote is located from Z_R at $\Phi = 29.22°$ ($\cos^2\Phi = (7 + 2\sqrt{46})/27$).

that one of eqs 4.3 corresponds to an imaginary surface. It follows that the + surface is a closed one (see for instance $\beta = 30°$ in Figure 10). Finally, it can be noted that the intersections of the averaged surfaces in the Z_R direction are given by

$$B(\boldsymbol{\beta})Z_R^4 = \pm 1 \qquad (4.5)$$

(the intersections can be imaginary).

Using eq 4.1, the intersection of the static surfaces in the Z_R direction corresponds to a radius R given by

$$(3/8)\sin^2\beta(8\cos^2\beta - \sin^2\beta)R^4 = \pm 1 \qquad (4.6a)$$

$$B(\boldsymbol{\beta})R^4 = \pm 1 \qquad (4.6b)$$

Equations 4.5 and 4.6b give a simple geometrical interpretation of Z_R; it corresponds simply to the intersection radius of the static surfaces in the rotor axis direction. Physically, it implies that no averaging occurs in the Z_R direction during rotation, whereas averaging occurs perpendicularly to this axis. We suppose now that B_o is oriented from the rapidly rotating rotor by the angle θ (see Figure 9). If $\theta = \zeta_m$, this situation corresponds to MAS. The intersection radius r_β of the averaged surfaces related to eqs 4.3 in the B_o direction is then given (for a fixed value of θ) by

$$\pm r_\beta^{-4} = A(\boldsymbol{\beta})\sin^4\theta + B(\boldsymbol{\beta})\cos^4\theta + C(\boldsymbol{\beta})\sin^2\theta\cos^2\theta \qquad (4.7)$$

$A(\boldsymbol{\beta})$, $B(\boldsymbol{\beta})$, and $C(\boldsymbol{\beta})$ are given in eqs 4.4. One can then derive easily the second-order shift under rapid rotation at θ for each crystallite's orientation as

$$\omega^{(2),\theta}_{-1/2,1/2} = C_{-1/2,1/2}\,(\pm r_\beta^{-4})$$

$$= C_{-1/2,1/2}\,(A(\boldsymbol{\beta})\sin^4\theta + B(\boldsymbol{\beta})\cos^4\theta + C(\boldsymbol{\beta})\sin^2\theta\cos^2\theta) \quad (4.8)$$

$C_{-1/2,1/2}$ is given by eq 2.15. For $\theta = \zeta_m$, eq 4.8 becomes

$$\omega^{(2),\zeta_m}_{-1/2,1/2} = (1/16)C_{-1/2,1/2}(21\cos^4\beta - 18\cos^2\beta + 5) \quad (4.9)$$

Equations 4.8 and 4.9 are strictly analogous to equations proposed in the literature.[25,32] At this stage, it is interesting to note that the quadrupolar shifts under VAS (eq 4.8) and MAS (eq 4.9) were easily derived by using the surfaces presented in Section 2. A clear pictorial representation is given. It is worth noting that the only prerequisite is the knowledge of the energy levels corrected by standard second-order perturbation theory (see Section 2). Equations 4.7−4.9 allow us to visualize the effects of VAS or MAS on the broadening of the central transition. $\omega^{(2),\theta}_{-1/2,1/2}$ is plotted versus β for various values of θ in Figure 11. The static second-order quadrupolar shift is also plotted, using eqs 2.19 and 2.21 and $(\pm r^{-4})_{\text{static}} = (3/8)\sin^2\beta_o\,(8\cos^2\beta_o - \sin^2\beta_o)$. For a fixed θ value, $|(\omega^{(2),\theta}_{-1/2,1/2})_{\max} - (\omega^{(2),\theta}_{-1/2,1/2})_{\min}|$ corresponds to the residual line width of the central transition. Most results concerning the MAS-VAS techniques are illustrated in Figure 11. (i) Reorientation at $\theta = 0°$ does not affect the static line width. In this case, $\beta = \beta_o$ and eq 4.8 becomes

$$\omega^{(2),0°}_{-1/2,1/2} = C_{-1/2,1/2}\,B(\boldsymbol{\beta}_o) = \omega^{(2),\text{static}}_{-1/2,1/2} \quad (4.10)$$

(see also eq 2.14). (ii) It appears that $[(\omega^{(2),\theta}_{-1/2,1/2})_{\max} - (\omega^{(2),\theta}_{-1/2,1/2})_{\min}]$ is never zero. In the MAS case, eq 4.9 leads to

$$(\omega^{(2),\zeta_m}_{-1/2,1/2})_{\max} = (1/14)C_{-1/2,1/2} \quad (4.11a)$$

for $\beta_{\max}$ given by $\cos^2\beta_{\max} = 3/7$ or $\beta_{\max} = 49.11°$ and to

$$(\omega^{(2),\zeta_m}_{-1/2,1/2})_{\min} = (1/2)C_{-1/2,1/2} \quad (4.11b)$$

for $\beta_{\min} = 0°$. Equations 4.11a and 4.11b are in agreement with results given in the literature. It is interesting to note that $\omega^{(2),\zeta_m}_{-1/2,1/2} < 0$, as $C_{-1/2,1/2} < 0$ for every β. It follows that the residual line is totally shifted apart from the true isotropic chemical shift. This is a general and well-known result. It can be understood geometrically by considering the Figure 10. The intersection of each curve in the B_o direction at $\theta = \zeta_m$ from Z_R exists for every β. It implies that $(+r_\beta^{-4})$ in eq 4.7 must be considered. (iii) The minimum residual line width is obtained for $\theta \approx 70°$. This result was also emphasized in the literature.[33]

The most important point concerning the MAS-VAS experiment is that no single-axis reorientation can totally remove the second-order broadening of the central transition. We shall demonstrate this important result just by using eqs 4.4 and 4.7. One can note that this approach will be used several times in the following sections. If rapid rotation at a particular value of θ allows the total suppression of the second-order broadening, it follows (eq 4.7) that

$$\pm r_\beta^{-4} = C_1 \quad (4.12)$$

C_1 being a constant *independent of* β. Equation 4.12 implies that

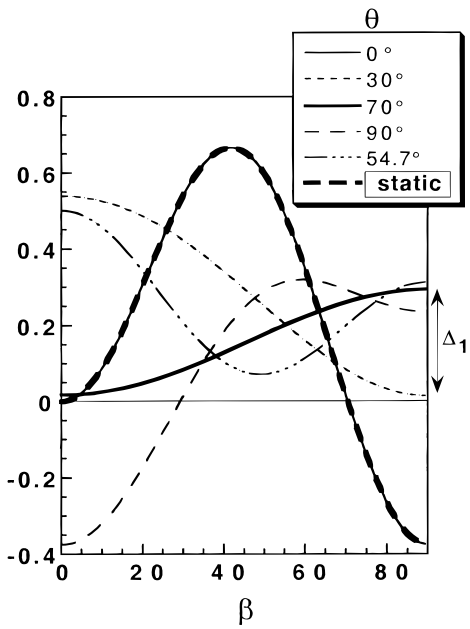

Figure 11. MAS-VAS experiment. Plot of $\omega^{(2),\theta}_{-1/2,1/2}$ versus β (see eq 4.8). The vertical axis is given in $C_{-1/2,1/2}$ units (eq 2.15). For a fixed θ value, $|(\omega^{(2),\theta}_{-1/2,1/2})_{\max} - (\omega^{(2),\theta}_{-1/2,1/2})_{\min}|$ corresponds to the residual line width. The minimum residual line width Δ_1 is obtained for $\theta \approx 70°$.

$$\frac{\partial}{\partial\beta}(\pm r_\beta^{-4}) = 0 \quad (4.13)$$

for every β (θ is fixed). Using eqs 4.4 and 4.7, eq 4.13 becomes

$$(27/16)S(\theta)\cos^3\beta - (3/16)T(\theta)\cos\beta = 0 \quad (4.14)$$

with

$$S(\theta) = 35\cos^4\theta - 30\cos^2\theta + 3 \quad (4.15a)$$

$$T(\theta) = 135\cos^4\theta - 102\cos^2\theta + 7 \quad (4.15b)$$

If eq 4.14 is fulfilled for every β, then the following equations must be fulfilled simultaneously:

$$S(\theta) = T(\theta) = 0;\ \theta \in [0,90°] \quad (4.16)$$

$S(\theta) = 0$ implies $\cos\theta = (3 \pm 2\sqrt{6/5})^{1/2}/\sqrt{7}$ or $\theta_+ = 30.56°$ and $\theta_- = 70.12°$. $T(\theta) = 0$ implies $\cos\theta = (17 \pm 2\sqrt{46})^{1/2}/(3\sqrt{5})$ or $\theta_+ = 34.50°$ and $\theta_- = 73.96°$. Obviously, the system of eqs 4.16 has no solution. It follows that no rotation at a given angle θ allows the total suppression of second-order broadening. At this stage, it can be noted that no explicit reference to the second- and fourth-order Legendre polynomials $P_2(\cos\theta)$ and $P_4(\cos\theta)$ was made. Netherveless, it can be realized that

$$S(\theta) = 8P_4(\cos\theta)$$

$$T(\theta) = (216/7)P_4(\cos\theta) + (64/7)P_2(\cos\theta) \quad (4.17)$$

with

$$P_2(\cos\theta) = (1/2)(3\cos^2\theta - 1) \quad (4.18a)$$

$$P_4(\cos\theta) = (1/8)(35\cos^4\theta - 30\cos^2\theta + 3) \quad (4.18b)$$

Solving the system 4.16 is then equivalent to finding a common root to $P_2(\cos\theta)$ and $P_4(\cos\theta)$. This is actually impossible and this statement has been widely used in the literature for the

interpretation of the MAS-VAS experiment dealing with quadrupolar nuclei.[16,34,35] However, it does not represent a key point of our discussion (see above).

Finally, we give generalized formulas for $\eta_Q \neq 0$. As stated in Section 2, the complementary fourth-degree surfaces accounting for the second-order broadening are given in the PAS by

$$aX^4 + bY^4 + cZ^4 + dX^2Y^2 + eX^2Z^2 + fY^2Z^2 = \pm 1 \quad (4.19)$$

$a-f$ are given in eqs 2.25 and are functions of η_Q. These surfaces are not necessarily of revolution. Following the calculations for $\eta_Q = 0$ presented above, the averaged fourth-degree surfaces are given in $(X_R Y_R Z_R)$ by

$$D(\alpha,\beta)\,(X_R^2 + Y_R^2)^2 + E(\alpha,\beta)Z_R^4 + F(\alpha,\beta)Z_R^2\,(X_R^2 + Y_R^2) = \pm 1 \quad (4.20)$$

with

$$D(\alpha,\beta) = -(9/64)[9-6\,\eta_Q(\cos 2\alpha) + \eta_Q^2(\cos 2\alpha)^2]\cos^4\beta + (1/32)\{21-40\eta_Q(\cos 2\alpha) + \eta_Q^2[2 + 9\,(\cos 2\alpha)^2]\}\cos^2\beta + (1/192)\{45 + 78\eta_Q(\cos 2\alpha) - \eta_Q^2[27(\cos 2\alpha)^2 - 16]\}$$

$$E(\alpha,\beta) = -(3/8)[9 - 6\eta_Q(\cos 2\alpha) + \eta_Q^2(\cos 2\alpha)^2]\cos^4\beta + (1/4)\{15 - 8\eta_Q(\cos 2\alpha) - \eta_Q^2[2 - 3(\cos 2\alpha)^2]\}\cos^2\beta - (1/24)\{9 + 6\eta_Q(\cos 2\alpha) + \eta_Q^2[9(\cos 2\alpha)^2 - 8]\}$$

$$F(\alpha,\beta) = -(9/8)[-9 + 6\eta_Q(\cos 2\alpha) - \eta_Q^2(\cos 2\alpha)^2]\cos^4\beta + (1/4)\{-33 + 32\eta_Q(\cos 2\alpha) + \eta_Q^2[2-9(\cos 2\alpha)^2]\}\cos^2\beta + (1/24)\{27 - 30\eta_Q(\cos 2\alpha) - \eta_Q^2[8 - 27(\cos 2\alpha)^2]\} \quad (4.21)$$

As stated above, the intersection radius $r_{\alpha,\beta}$ of the averaged surfaces related to eq 4.20 in the B_o direction is then given by

$$\pm r_{\alpha,\beta}^{-4} = D(\alpha,\beta)\sin^4\theta + E(\alpha,\beta)\cos^4\theta + F(\alpha,\beta)\sin^2\theta\cos^2\theta \quad (4.22)$$

for a fixed θ value.

The second-order shift under rapid rotation at θ for each crystallite's orientation is then given by

$$\omega_{-1/2,1/2}^{(2),\theta} = C_{-1/2,1/2}(\pm r_{\alpha,\beta}^{-4})$$

$$= C_{-1/2,1/2}\,(D(\alpha,\beta)\sin^4\theta + E(\alpha,\beta)\cos^4\theta + F(\alpha,\beta)\sin^2\theta\cos^2\theta) \quad (4.23)$$

$C_{-1/2,1/2}$ is given in eq 2.15. For $\theta = \zeta_m$, (that is, MAS), eq 4.23 becomes

$$\omega_{-1/2,1/2}^{(2),\zeta_m} = C_{-1/2,1/2}\,\{[21/16-(7/8)\eta_Q(\cos 2\alpha) + (7/48)\eta_Q^2(\cos 2\alpha)^2]\cos^4\beta + [-9/8 + (1/12)\eta_Q^2 + \eta_Q(\cos 2\alpha) - (7/24)\eta_Q^2(\cos 2\alpha)^2]\cos^2\beta + [5/16 - (1/8)\eta_Q(\cos 2\alpha) + (7/48)\eta_Q^2(\cos 2\alpha)^2]\} \quad (4.24)$$

Equations 4.23 and 4.24 are in agreement with those proposed in the literature.[25] Again, it should be noted that they are derived easily and connected directly to the averaged fourth-degree surfaces related to eq 4.20.

The effect of the MAS-VAS experiment on dipolar coupled $I-S$ systems ($S > 1/2$) (see Section 3) will now be presented. Representative surfaces of this particular interaction are given by eqs 3.2. As presented above and using the integrals $I_{r,s}$ (see eq 4.2 and Table 2), averaged surfaces can be defined under rapid rotation for every m_s value. These averaged surfaces for $m_s = 0, +1, -1$ are given in $(X_R Y_R Z_R)$ by

$$G_{m_s}(\beta)(X_R^2 + Y_R^2)^2 + H_{m_s}(\beta)Z_R^4 + I_{m_s}(\beta)Z_R^2(X_R^2 + Y_R^2) \pm 1 \quad (4.25)$$

with

$$G_{m_s}(\beta) = (3/8)(a_{m_s} + b_{m_s} - c_{m_s})\cos^4\beta + (1/4)(a_{m_s} - 3b_{m_s} + c_{m_s})\cos^2\beta + (1/8)(3a_{m_s} + 3b_{m_s} + c_{m_s})$$

$$H_{m_s}(\beta) = (a_{m_s} + b_{m_s} - c_{m_s})\cos^4\beta + (-2a_{m_s} + c_{m_s})\cos^2\beta + a_{m_s}$$

$$I_{m_s}(\beta) = -3(a_{m_s} + b_{m_s} - c_{m_s})\cos^4\beta + (2a_{m_s} + 3b_{m_s} - (5/2)c_{m_s})\cos^2\beta + (a_{m_s} + (1/2)c_{m_s}) \quad (4.26)$$

The a_{m_S}, b_{m_S}, and c_{m_S} coefficients are given in Table 1. We suppose that B_o is oriented from the rapidly rotating rotor by the angle θ. The intersection radius r_β of the averaged surfaces (eqs 4.25) in the B_o direction is given by

$$\pm r_\beta^{-4} = G_{m_s}(\beta)\sin^4\theta + H_{m_s}(\beta)\cos^4\theta + I_{m_s}(\beta)\cos^2\theta\sin^2\theta \quad (4.27)$$

For $\theta = \zeta_m$ (that is, MAS), one obtains under rapid rotation

$$\omega_0^{\zeta_m} = c_o/18\,(7\cos^4\beta - 6\cos^2\beta + 3) \quad (4.28a)$$

$$\omega_{+1}^{\zeta_m} = \omega_{-1}^{\zeta_m} = -(\omega_0^{\zeta_m})/2 \quad (4.28b)$$

It is obvious that rapid MAS cannot suppress completely the involved interaction and that a residual line width will be observed. Again, if rapid rotation at a particular value of θ allows the total suppression of the broadening, it follows (using eq 4.27) that

$$\pm r_\beta^{-4} = C_2 \quad (4.29)$$

with C_2 being a constant independent of β. Using eq 4.13, one obtains the following equation:

$$U(\theta)\cos^3\beta - (1/2)V(\theta)\cos\beta = 0 \quad (4.30)$$

with

$$U(\theta) = (1/2)S(\theta)$$

$$V(\theta) = 15\cos^4\theta - 12\cos^2\theta + 1 = (3/16)S(\theta) + (1/16)T(\theta) \quad (4.31)$$

$S(\theta)$ and $T(\theta)$ are given by eqs 4.15. As eq 4.30 must be valid for every β, θ must fulfill $U(\theta) = V(\theta) = 0$ and $\theta \in [0,90°]$. $U(\theta) = 0$ implies $\theta_+ = 30.56°$ and $\theta_- = 70.12°$. $V(\theta) = 0$

implies $\cos\theta = (6 \pm \sqrt{21})^{1/2}/\sqrt{15}$ or $\theta_+ = 32.87°$ and $\theta_- = 72.09°$. It follows that no rotation at a given θ allows the total suppression of the dipolar interaction. It can further be noted that

$$U(\theta) = 4P_4(\cos\theta)$$

$$V(\theta) = (24/7)P_4(\cos\theta) + (4/7)P_2(\cos\theta) \quad (4.32)$$

$P_2(\cos\theta)$ and $P_4(\cos\theta)$ are defined by eqs 4.18. The situation presented here is therefore strictly analogous to that presented above and related to the (−1/2,1/2) central transition of quadrupolar nuclei.

5. Dynamic-Angle Spinning, Dynamic-Angle Hopping and Double Rotation

It has been demonstrated theoretically and experimentally, in the late 1980s,[17−19] that the total suppression of second-order broadening was actually possible. Rapid rotation around two axes at particular angles θ_1 and θ_2 (that is DAS) yields a 2D correlation. One dimension is related to the "isotropic" dimension and in this sense, high resolution for quadrupolar nuclei is attained. Each DAS angles pair is connected to a factor k, which connects the time at θ_1 and the time at θ_2. In connection with the DAS experiment, another experimental scheme was proposed for the total suppression of second-order broadening effects,[20,21] the double-rotation of samples. A small inner rotor (rotor 1) is rotating in a rotating outer rotor (rotor 2). For particular values of θ_i (the angle between the inner and the outer rotor) and θ_e (the angle between the outer rotor and B_o), isotropic lines are obtained for each distinct crystallographic site.

We give now a pictorial representation of the DAS experiment. We consider the averaged surfaces presented in Figure 10 and described by eqs 4.3 and 4.4. The intersections of these surfaces in the B_o direction at θ_1 and θ_2 are given by eq 4.7 and lead to two $\omega^{(2),\theta_1}_{-1/2,1/2}$ and $\omega^{(2),\theta_2}_{-1/2,1/2}$ values. For a given (θ_1, θ_2, k) set, and if high resolution is attained, the following equation must be fulfilled:

$$(\pm r_\beta^{-4})^{\theta_1^\circ} + k(\pm r_\beta^{-4})^{\theta_2^\circ} = C_3 \quad (5.1)$$

C_3 being a constant independent of β. Using eqs 4.13−4.15, it follows that

$$(27/16)[S(\theta_1) + kS(\theta_2)]\cos^3\beta - (3/16)[T(\theta_1) + kT(\theta_2)]\cos\beta = 0 \quad (5.2)$$

$S(\theta)$ and $T(\theta)$ are given by eqs 4.15. It follows that

$$S(\theta_1) + kS(\theta_2) = 0 \quad (5.3a)$$

$$T(\theta_1) + kT(\theta_2) = 0 \quad (5.3b)$$

This system can be analytically resolved, leading to

$$\theta_1 = \arccos\left[\frac{1}{3}\left(1 + \frac{2\sqrt{k}}{\sqrt{5}}\right)\right]^{1/2}$$

$$\theta_2 = \arccos\left[\frac{-2\sqrt{5} + 5\sqrt{k}}{15\sqrt{k}}\right]^{1/2}$$

$$4/5 \le k \le 5 \quad (5.4)$$

These analytical solutions are in agreement with those proposed in the literature.[36] Using eqs 4.4, 4.8, and 5.4 and $\beta = 90°$ (as the following quantity is now independent of β), one obtains immediatly

$$(\omega^{(2),\theta_1^\circ}_{-1/2,1/2} + k\omega^{(2),\theta_2^\circ}_{-1/2,1/2})/(1+k) = (1/5)C_{-1/2,1/2} \quad (5.5)$$

High resolution is attained and the isotropic shift is given by ($\eta_Q = 0$)

$$\omega^{(2),\mathrm{iso}}_{-1/2,1/2} = (1/5)C_{-1/2,1/2} = -\frac{4\pi^2}{30\omega_0}\left[\frac{3C_Q}{2I(2I-1)}\right]^2[I(I+1) - 3/4] \quad (5.6)$$

It was first demonstrated by Gann and co-workers[37] that continuous rotation of samples around the (θ_1, θ_2) DAS angles is not necessary. Regular "hops" at θ_1 and θ_2 are indeed sufficient. We follow our approach of surfaces averaging (see Section 4). Rapid rotation implies averaging of trigonometric terms, leading to the integrals $I_{r,s}$ (see eq 4.2) with $(r+s) \le 4$. If averaging is possible by discrete regular p "hops" of the rotor at a given angle, then one must fulfill the following equations:

$$I_{r,s} = 1/p\sum_{q=0}^{p-1}\left[\cos\left(\gamma + q\frac{360}{p}\right)\right]^r\left[\sin\left(\gamma + q\frac{360}{p}\right)\right]^s \quad (5.7)$$

for every (r, s) and every γ. Simple trigonometric calculations show that $p = 5$ corresponds to the minimal value. The successive "hops" of the rotor describe a regular pentagon. Generally, 10 orientations of the rotor are thus necessary for a given (θ_1, θ_2) DAS angles pair (five positions at θ_1 with 72° increments and five positions at θ_2 with the same increments). However, the minimum number is six. Indeed, for $\theta_1 = 0°$, the shift under rapid rotation corresponds to the intersection of the *static* fourth-degree surface (as for $\theta_1 = 0°$, the rotor axis and B_o are collinear). It follows that one position at $\theta_1 = 0°$ and five positions at $\theta_2 = 63.43°$ are sufficient to fulfill the criteria of a DAH experiment. In their original work, Gann and co-workers used the (0°, 63.43°) pair for sensitivity considerations.[37] It is interesting to note that this hopping averaging procedure is an extension of MAH, devoted to first-order interactions.[38] In this particular case, $(r+s) \le 2$ (see ref 10 for a pictorial representation of MAH).

Finally, averaged surfaces related to a DOR experiment can be obtained. As stated above, the criteria for high resolution lead to a system of equations involving θ_i and θ_e. This system can be analytically solved, leading to the various (θ_i, θ_e) angles pairs. They correspond to roots of $P_2(\cos\theta)$ and $P_4(\cos\theta)$.[35,39]

6. Multiple-Quantum Magic-Angle Spinning and Multiple-Quantum Variable-Angle Spinning

In Section 5, we have presented a pictorial approach of DAS, DAH, and DOR experiments. In particular, we have shown that the exact calculation of the second-order isotropic shift could be easily derived, by using averaged fourth-degree surfaces. However, DAS and DOR remain demanding experiments, as special probes (including for instance rapid rotation axis flipping in DAS or mutual rotation of two rotors in DOR) are required. Moreover, spin dynamics considerations or appearance of numerous spinning sidebands have limited so far a "routine" use of these experiments. However, the concept of DAS and DOR was very fruitful. Indeed, it was demonstrated that for the total suppression of second-order broadening, a second degree of freedom is needed (in contrast with MAS, which involves rotation around a single axis). Recently, Frydman and

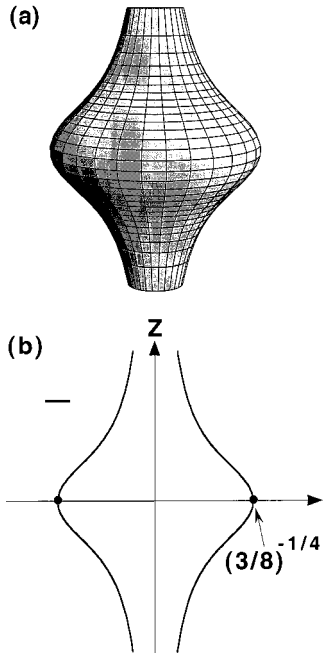

Figure 12. (a) Pictorial representation of the triple-quantum coherence ($I = 3/2$) corresponding to the equation $-(3/8)(X^2 + Y^2)[8Z^2 + (X^2 + Y^2)] = -1$ (eq 6.6, $\eta_Q = 0$). The Z axis of the PAS corresponds to the axis of revolution and to an asymptote. (b) Section of the surface by any plane containing the Z axis. The sign $-$ is emphasized.

co-workers have demonstrated theoretically and experimentally that the total suppression of second-order broadening was possible by using a standard MAS probe.[22,23] The second degree of freedom is chosen in the multiple-quantum coherences of the quadrupolar energy levels system. The MQ-MAS experiment had a great impact in the field of quadrupolar nuclei. To our knowledge, more articles involving the MQ-MAS experiment[22,23,40] were published during the last three years than articles dealing with DAS or DOR (over a decade period). We propose now a pictorial representation of multiple-quantum (MQ) transitions and MQ-MAS experiment. At first insight, it seems rather difficult to illustrate the MQ coherences. If these illustrations are found, the MQ-MAS experiment will then be interpreted in terms of correlation between the MQ transitions and the (−1/2,1/2) transition. In the following, the $I = 3/2$ and $I = 5/2$ cases will be treated in detail. Let us suppose first $I = 3/2$ and $\eta_Q = 0$. The expression of the central transition shift involving second-order effects is given by eq 2.14

$$\omega^{(2),\mathrm{static}}_{-1/2,1/2} = C_{-1/2,1/2}[(3/8)\sin^2\beta_o(9\cos^2\beta_o - 1)] + \omega_{cs} \quad (6.1)$$

$C_{-1/2,1/2}$ is given by eq 2.15. In eq 6.1, we introduce explicitly ω_{cs}, which includes the "true" chemical shift of the considered nucleus. Considering $I = 3/2$, eq 6.1 can be rewritten as

$$\omega^{(2),\mathrm{static}}_{-1/2,1/2} = C^{3/2}[(3/8)\sin^2\beta_o(9\cos^2\beta_o - 1)] + \omega_{cs} \quad (6.2)$$

$$C^{3/2} = -\frac{2\pi^2}{\omega_o}\left[\frac{3C_Q}{2I(2I-1)}\right]^2 \quad (6.3)$$

We now decide to describe the triple-quantum coherence by the following equation (using eqs 2.5):

$$\omega^{(2),\mathrm{static},3/2}_{-3/2,3/2} = \hbar^{-1}(E^{(2)}_{-3/2} - E^{(2)}_{3/2}) + 3\omega_{cs} \quad (6.4)$$

Inserting the constant $C^{3/2}$, one obtains

$$\omega^{(2),\mathrm{static},3/2}_{-3/2,3/2} = C^{3/2}[-(3/8)\sin^2\beta_o(7\cos^2\beta_o + 1)] + 3\omega_{cs} \quad (6.5)$$

We focus first on the geometrical terms involving β_o in eqs 6.2 and 6.5. A representation of $\omega^{(2),\mathrm{static}}_{-1/2,1/2}$ is given by eqs 2.19, 2.21 and Figures 3−4. A direct representation of $\omega^{(2),\mathrm{static},3/2}_{-3/2,3/2}$ is then given by the fourth-degree surfaces

$$-(3/8)(X^2 + Y^2)[8Z^2 + (X^2 + Y^2)] = \pm 1 \quad (6.6)$$

Obviously, one of these surfaces is imaginary. These equations are of revolution with the Z axis as the axis of revolution. The surface corresponding to $-(3/8)(X^2 + Y^2)[8Z^2 + (X^2 + Y^2)] = -1$ is presented in Figure 12, as well as the intersection of the surface by any plane containing the Z axis. The sign $-$ is emphasized. The second step in the description of the MQ-MAS experiment is the transformation of the surfaces described above under rapid rotation. For the central transition, averaged surfaces are given by eqs 4.3−4.4. Following the procedure described in Section 4, the averaged surfaces corresponding to the triple-quantum coherence are then given by

$$A^{3/2}_{-3/2,3/2}(X_R^2 + Y_R^2)^2 + B^{3/2}_{-3/2,3/2}Z_R^4 + C^{3/2}_{-3/2,3/2}Z_R^2(X_R^2 + Y_R^2) = \pm 1 \quad (6.7)$$

with

$$A^{3/2}_{-3/2,3/2} = (3/64)(21\cos^4\beta - 18\cos^2\beta - 11)$$

$$B^{3/2}_{-3/2,3/2} = (3/8)(7\cos^4\beta - 6\cos^2\beta - 1)$$

$$C^{3/2}_{-3/2,3/2} = (3/8)(-21\cos^4\beta + 18\cos^2\beta - 5) \quad (6.8)$$

β corresponds to the angle between the Z axis of the quadrupolar PAS and the Z_R axis of the rotor. Under rapid MAS ($\theta = \zeta_m$), the corresponding shifts are derived and correspond to the intersections of the surfaces described above in the B_o direction.

$$(\pm r_\beta^{-4})_{-1/2,1/2} = A(\boldsymbol{\beta})\sin^4\zeta_m + B(\boldsymbol{\beta})\cos^4\zeta_m + C(\boldsymbol{\beta})\sin^2\zeta_m\cos^2\zeta_m = (4/9)A(\boldsymbol{\beta}) + (1/9)B(\boldsymbol{\beta}) + (2/9)C(\boldsymbol{\beta}) \quad (6.9a)$$

$$(\pm r_\beta^{-4})^{3/2}_{-3/2,3/2} = A^{3/2}_{-3/2,3/2}\sin^4\zeta_m + B^{3/2}_{-3/2,3/2}\cos^4\zeta_m + C^{3/2}_{-3/2,3/2}\sin^2\zeta_m\cos^2\zeta_m = (4/9)A^{3/2}_{-3/2,3/2} + (1/9)B^{3/2}_{-3/2,3/2} + (2/9)C^{3/2}_{-3/2,3/2} \quad (6.9b)$$

$A(\boldsymbol{\beta})$, $B(\boldsymbol{\beta})$, and $C(\boldsymbol{\beta})$ are given in eqs 4.4. The MQ-MAS experiment can be interpreted as an evolution under $\omega^{(2),\zeta_m}_{-3/2,3/2}$ followed by an evolution during t_e under $\omega^{(2),\zeta_m}_{-1/2,1/2}$. If high resolution is attained, the following equation must be fulfilled:

$$(\pm r_\beta^{-4})^{3/2}_{-3/2,3/2} + t_e(\pm r_\beta^{-4})_{-1/2,1/2} = C_4 \quad (6.10)$$

with C_4 being a constant independent of β. It follows that $\partial/\partial\beta[(\pm r_\beta^{-4})^{3/2}_{-3/2,3/2} + t_e(\pm r_\beta^{-4})_{-1/2,1/2}] = 0$ or

$$(7/24)(9t_e - 7)\cos^3\beta + (1/8)(7 - 9t_e)\cos\beta = 0 \quad (6.11)$$

Equation 6.11 is fulfilled for every β if $t_e = 7/9$. In other words, an echo coded by an isotropic shift is obtained for $t_e = 7/9$. This is a direct representation of the MQ-MAS experiment. It is crucial to note that we have illustrated in this case the so-

called ($-3Q$) echo (this notation is now usual in the literature[41]). Indeed, it corresponds to the difference ($E^{(2)}_{-3/2} - E^{(2)}_{3/2}$) (see eq 6.4) and *not* to the opposite. If ($E^{(2)}_{3/2} - E^{(2)}_{-3/2}$) is used, eq 6.11 is slightly modified and becomes

$$(49/3 + 21t_e)\cos^3\beta + (1/8)(7 + 9t_e)\cos\ \beta = 0 \qquad (6.12)$$

Equation 6.12 is fulfilled for every β if $t_e = -7/9$ (i.e., in the "negative" time domain). The constant C_4 can be readily calculated for a particular value of β (that is, $\beta = 90°$) by using eq 6.10 and $t_e = 7/9$. One obtains

$$C^{3/2}C_4 = (4/9)\frac{2\pi^2}{\omega_o}\left[\frac{3C_Q}{2I(2I-1)}\right]^2 = -(20/9)\omega^{(2),iso}_{-1/2,1/2} \qquad (6.13)$$

($\omega^{(2),iso}_{-1/2,1/2}$ is given by eq 5.6). It is important to note that eqs 6.2 and 6.4 contain some terms involving the true chemical shift ω_{cs}. This contribution can be easily described by the following surfaces:

$$\omega_{cs}(X^2 + Y^2 + Z^2)^2 = 1 \qquad (6.14a)$$

$$3\omega_{cs}\,(X^2 + Y^2 + Z^2)^2 = 1 \qquad (6.14b)$$

as $(r^{-4}) = \omega_{cs}$ and $(r^{-4}) = 3\omega_{cs}$, respectively. The eqs 6.14a and 6.14b correspond to surfaces having the shape of spheres of radius $(\omega_{cs})^{-1/4}$ and $(3\omega_{cs})^{-1/4}$ (we suppose $\omega_{cs} > 0$). They are invariant under rapid rotation and the evolution under the three-quantum coherence followed by the single-quantum coherence is thus given by

$$3\omega_{cs} + t_e\omega_{cs} = (34/9)\omega_{cs} \qquad (6.15)$$

assuming that $t_e = 7/9$ (see above). It follows that the attained isotropic shift (when performing a MQ-MAS experiment) contains two terms:

$$\omega^{(2),iso,3/2}_{-3/2,3/2} = -(20/9)\omega^{(2),iso}_{-1/2,1/2} + (34/9)\omega_{cs} \qquad (6.16)$$

This formula is in agreement with that proposed in the literature.[41] Other equivalent formulas can be found in the literature.[23] It has thus been demonstrated that simple fourth-degree surfaces are able to illustrate the main results of the MQ-MAS experiment. At this stage, several comments can be made. The MQ-MAS experiment is comparable to the DAS experiment. However, in DAS, the second-order isotropic shift ($\omega^{(2),iso}_{-1/2,1/2}$) is analytically obtained after *weighting* of the shifts at θ_1 and θ_2 ((θ_1, θ_2) corresponding to a DAS angles pair) (see eq 5.5). On the contrary, the derivation of the second-order shift in MQ-MAS ($\omega^{(2),iso,3/2}_{-3/2,3/2}$) does not involve any weighting (see eq 6.10). This proves that DAS and MQ-MAS are not strictly analogous. Anyway, both methodologies lead to a 2D experiment involving an isotropic and an anisotropic dimension and are comparable in this sense. Second, eq 6.11 shows that the only echo containing an isotropic information is obtained for $t_e = 7/9$. The location of other echoes is predicted,[41] but they cannot contain any isotropic information as shown by eq 6.11. Finally, it is rather surprising to note that the triple-quantum coherence can be illustrated by the simple difference of the corresponding energy levels (see eq 6.4). In particular, the quantity ($3\omega_{cs}$) is involved. It is crucial to note that this term does not correspond to an irradiation at ($3\omega_o$) but irradiation at ω_o. Nethertheless, ($3\omega_{cs}$) and ω_{cs} allow us to derive the shift of the true chemical shift (see eqs 6.15 and 6.16). We now turn to the case $I = 5/2$. Again, the central transition is characterized by

$$\omega^{(2),static}_{-1/2,1/2} = C^{5/2}\,[(3/8)\sin^2\beta_o(9\cos^2\beta_o - 1)] + \omega_{cs} \qquad (6.17)$$

$$C^{5/2} = -\frac{16}{3}\frac{\pi^2}{\omega_o}\left[\frac{3C_Q}{2I(2I-1)}\right]^2 \qquad (6.18)$$

Using eq 2.5, the triple-quantum coherence (corresponding to ($+3Q$)) is then given by

$$\omega^{(2),static,5/2}_{3/2,-3/2} = \hbar^{-1}(E^{(2)}_{3/2} - E^{(2)}_{-3/2}) - 3\omega_{cs} \qquad (6.19)$$

We note that this equation corresponds to the opposite of eq 6.4. Indeed, the ($+3Q$) coherence is involved here. Inserting the constant $C^{5/2}$, one obtains

$$\omega^{(2),static,5/2}_{3/2,-3/2} = C^{5/2}\,[(27/32)\sin^2\beta_o(\sin^2\beta_o - (16/3)\cos^2\beta_o)] - 3\omega_{cs} \qquad (6.20)$$

A representation of the geometrical part of $\omega^{(2),static,5/2}_{3/2,-3/2}$ is then given by

$$(27/32)(X^2 + Y^2)[-(16/3)Z^2 + (X^2 + Y^2)] = \pm 1 \qquad (6.21)$$

Under rapid rotation, these equations become

$$A^{5/2}_{+3/2,-3/2}(X^2 + Y^2)^2 + B^{5/2}_{+3/2,-3/2}Z^4 + C^{5/2}_{+3/2,-3/2}Z^2(X^2 + Y^2) = \pm 1 \qquad (6.22)$$

with

$$A^{5/2}_{+3/2,-3/2} = (3/256)(171\cos^4\beta - 78\cos^2\beta - 21)$$

$$B^{5/2}_{+3/2,-3/2} = (3/32)(57\cos^4\beta - 66\cos^2\beta + 9)$$

$$C^{5/2}_{+3/2,-3/2} = (3/32)(-171\cos^4\beta + 138\cos^2\beta - 15) \qquad (6.23)$$

When $\theta = \zeta_m$, the shifts are given by

$$(\pm r_\beta^{-4})_{-1/2,1/2} = (4/9)A(\boldsymbol{\beta}) + (1/9)B(\boldsymbol{\beta}) + (2/9)C(\boldsymbol{\beta}) \qquad (6.24a)$$

$$(\pm r_\beta^{-4})^{5/2}_{+3/2,-3/2} = (4/9)A^{5/2}_{+3/2,-3/2} + (1/9)B^{5/2}_{+3/2,-3/2} + (2/9)C^{5/2}_{+3/2,-3/2} \qquad (6.24b)$$

(see eqs 4.4 and 6.9). The condition for high resolution is given by $(\pm r_\beta{}^{-4})^{5/2}_{+3/2,-3/2} + t_e(\pm r_\beta{}^{-4})_{-1/2,1/2} = C_5$, with C_5 being a constant. It leads to the following equation:

$$2(-133/64 + (21/16)t_e)\cos^3\beta + (57/32 - (9/8)t_e)\cos\beta = 0 \qquad (6.25)$$

An echo occurs at $t_e = 19/12$. The constant C_5 is then calculated for $\beta = 90°$. One obtains

$$C^{5/2}\,C_5 = -(8/9)\frac{\pi^2}{\omega_o}\left[\frac{3C_Q}{2I(2I-1)}\right]^2 = (5/6)\omega^{(2),iso}_{-1/2,1/2} \qquad (6.26)$$

As stated above (eq 6.15),

$$-3\omega_{cs} + t_e\omega_{cs} = -(17/12)\,\omega_{cs} \qquad (6.27)$$

assuming $t_e = 19/12$. The attained isotropic shift is therefore

TABLE 3: Principal Features for the Representation of Multiple-Quantum Transitions and the MQ-MAS Experiment[a]

***I* = 3/2**	$C^{3/2} = -(2\pi^2/\omega_o)\,\epsilon$	***I* =7/2**	$C^{7/2} = -(10\pi^2/\omega_o)\,\epsilon$
	−3Q		***+3Q***
	$\omega^{st}_{-3} = -(3/8)\sin^2\beta_o\,(8\cos^2\beta_o+\sin^2\beta_o) + 3\omega_{cs}/C^{3/2}$		$\omega^{st}_{+3} = (3/40)\sin^2\beta_o\,(-88\cos^2\beta_o+13\sin^2\beta_o) - 3\omega_{cs}/C^{7/2}$
	$-(3/8)\,(X^2+Y^2)\,[8Z^2+(X^2+Y^2)] = \pm 1$*		$(3/40)\,(X^2+Y^2)\,[-88Z^2+13(X^2+Y^2)] = \pm 1$
	$A_{-3} = (3/64)\,(21\cos^4\beta-18\cos^2\beta-11)$		$A_{+3} = (3/320)\,(303\cos^4\beta-150\cos^2\beta-49)$
	$B_{-3} = (3/8)\,(7\cos^4\beta-6\cos^2\beta-1)$		$B_{+3} = (3/40)\,(101\cos^4\beta-114\cos^2\beta+13)$
	$C_{-3} = (3/8)\,(-21\cos^4\beta+18\cos^2\beta-5)$		$C_{+3} = (3/40)\,(-303\cos^4\beta+246\cos^2\beta-31)$
	$t_e = 7/9$		$t_e = 101/45$
	$\omega^{iso}_{-3} = -(20/9)\,\omega^{iso} + (34/9)\,\omega_{cs}$		$\omega^{iso}_{+3} = (4/9)\,\omega^{iso} - (34/45)\,\omega_{cs}$
***I* = 5/2**	$C^{5/2} = -(16/3)(\pi^2/\omega_o)\,\epsilon$		***+5Q***
	+3Q		$\omega^{st}_{+5} = (1/8)\sin^2\beta_o\,(-24\cos^2\beta_o+9\sin^2\beta_o) - 5\omega_{cs}/C^{7/2}$
	$\omega^{st}_{+3} = (27/32)\sin^2\beta_o\,(-16/3\,\cos^2\beta_o+\sin^2\beta_o) - 3\omega_{cs}/C^{5/2}$		$(1/8)\,(X^2+Y^2)\,[-24Z^2+9(X^2+Y^2)] = \pm 1$
	$(27/32)\,(X^2+Y^2)\,[-16/3\,Z^2+(X^2+Y^2)] = \pm 1$		$A_{+5} = (3/64)\,(33\cos^4\beta-10\cos^2\beta+1)$
	$A_{+3} = (3/256)\,(171\cos^4\beta-78\cos^2\beta-21)$		$B_{+5} = (3/8)\,(11\cos^4\beta-14\cos^2\beta+3)$
	$B_{+3} = (3/32)\,(57\cos^4\beta-66\cos^2\beta+9)$		$C_{+5} = (3/8)\,(-33\cos^4\beta+26\cos^2\beta-1)$
	$C_{+3} = (3/32)\,(-171\cos^4\beta+138\cos^2\beta-15)$		$t_e = 11/9$
	$t_e = 19/12$		$\omega^{iso}_{+5} = (20/9)\,\omega^{iso} - (34/9)\,\omega_{cs}$
	$\omega^{iso}_{+3} = (5/6)\,\omega^{iso} - (17/12)\,\omega_{cs}$		
	−5Q		***−7Q***
	$\omega^{st}_{-5} = -(15/32)\sin^2\beta_o\,(16\cos^2\beta_o+\sin^2\beta_o) + 5\omega_{cs}/C^{5/2}$		$\omega^{st}_{-7} = -(1/5)\sin^2\beta_o\,(63\cos^2\beta_o+21/8\,\sin^2\beta_o) + 7\omega_{cs}/C^{7/2}$
	$-(15/32)\,(X^2+Y^2)\,[16\,Z^2+(X^2+Y^2)] = \pm 1$*		$-(1/5)\,(X^2+Y^2)\,[63Z^2+21/8\,(X^2+Y^2)] = \pm 1$*
	$A_{-5} = (3/256)\,(225\cos^4\beta-170\cos^2\beta-95)$		$A_{-7} = (3/320)\,(483\cos^4\beta-350\cos^2\beta-189)$
	$B_{-5} = (3/32)\,(75\cos^4\beta-70\cos^2\beta-5)$		$B_{-7} = -(3/40)\,(-161\cos^4\beta+154\cos^2\beta+7)$
	$C_{-5} = (3/32)\,(-225\cos^4\beta+190\cos^2\beta-45)$		$C_{-7} = (3/40)\,(-483\cos^4\beta+406\cos^2\beta-91)$
	$t_e = 25/12$		$t_e = 161/45$
	$\omega^{iso}_{-5} = -(25/6)\,\omega^{iso} + (85/12)\,\omega_{cs}$		$\omega^{iso}_{-7} = -(56/9)\,\omega^{iso} + (476/45)\,\omega_{cs}$
***I* = 9/2**	$C^{9/2} = -(16\pi^2/\omega_o)\,\epsilon$		***+7Q***
	+3Q		$\omega^{st}_{+7} = (21/16)\,\sin^4\beta_o - 7\omega_{cs}/C^{9/2}$
	$\omega^{st}_{+3} = (1/32)\,\sin^2\beta_o\,(-240\cos^2\beta_o+33\sin^2\beta_o) - 3\omega_{cs}/C^{9/2}$		$(21/16)\,(X^2+Y^2)^2 = \pm 1$*
	$(1/32)\,(X^2+Y^2)\,[-240Z^2+33(X^2+Y^2)] = \pm 1$		$A_{+7} = (1/128)\,(63\cos^4\beta+42\cos^2\beta+63)$
	$A_{+3} = (1/256)\,(819\cos^4\beta-414\cos^2\beta-141)$		$B_{+7} = (21/16)\,(\cos^4\beta-2\cos^2\beta+1)$
	$B_{+3} = (1/32)\,(273\cos^4\beta-306\cos^2\beta+33)$		$C_{+7} = (1/16)\,(-63\cos^4\beta+42\cos^2\beta+21)$
	$C_{+3} = (1/32)\,(-819\cos^4\beta+666\cos^2\beta-87)$		$t_e = 7/18$
	$t_e = 91/36$		$\omega^{iso}_{+7} = (35/9)\,\omega^{iso} - (119/18)\,\omega_{cs}$
	$\omega^{iso}_{+3} = (5/18)\,\omega^{iso} - (17/36)\,\omega_{cs}$		
	+5Q		***−9Q***
	$\omega^{st}_{+5} = (1/32)\,\sin^2\beta_o\,(-240\,\cos^2\beta_o+45\sin^2\beta_o) - 5\omega_{cs}/C^{9/2}$		$\omega^{st}_{-9} = -(9/16)\,\sin^2\beta_o\,(32\cos^2\beta_o+\sin^2\beta_o) + 9\omega_{cs}/C^{9/2}$
	$(1/32)\,(X^2+Y^2)\,[-240Z^2+45(X^2+Y^2)] = \pm 1$		$-(9/16)\,(X^2+Y^2)\,[32Z^2+(X^2+Y^2)] = \pm 1$*
	$A_{+5} = (1/256)\,(855\cos^4\beta-390\cos^2\beta-105)$		$A_{-9} = (1/128)\,(837\cos^4\beta-594\cos^2\beta-315)$
	$B_{+5} = (1/32)\,(285\cos^4\beta-330\cos^2\beta+45)$		$B_{-9} = (1/16)\,(279\cos^4\beta-270\cos^2\beta-9)$
	$C_{+5} = (1/32)\,(-855\cos^4\beta+690\cos^2\beta-75)$		$C_{-9} = (1/16)\,(-837\cos^4\beta+702\cos^2\beta-153)$
	$t_e = 95/36$		$t_e = 31/6$
	$\omega^{iso}_{+5} = (25/18)\,\omega^{iso} - (85/36)\,\omega_{cs}$		$\omega^{iso}_{-9} = -(25/3)\,\omega^{iso} + (85/6)\,\omega_{cs}$

[a] For clarity: $\epsilon = [3C_Q/2I(2I-1)]^2$, related to the constant $C^{I=n/2}$; $\omega^{st}_{\pm m} \equiv (\omega^{(2),static,I=n/2}_{\pm m/2,\mp m/2})/C^{I=n/2}$, related to the "static" fourth-degree surfaces; $A_{\pm m} \equiv A^{I=n/2}_{\pm m/2,\mp m/2}$ (as well as for $B_{\pm m}$ and $C_{\pm m}$), related to the averaged fourth-degree surfaces under rapid rotation; $\omega^{iso}_{\pm m} \equiv \omega^{(2),iso,I=n/2}_{\pm m/2,\mp m/2}$, related to the quadrupolar isotropic shift; $\omega^{iso} \equiv \omega^{(2)iso}_{-1/2,1/2}$, related to the quadrupolar isotropic shift of the central transition; ω_{cs} corresponds to the true isotropic chemical shift. * indicates that one of the considered surfaces is imaginary.

given by

$$\omega^{(2),iso,5/2}_{+3/2,-3/2} = (5/6)\omega^{(2),iso}_{-1/2,1/2} - (17/12)\omega_{cs} \qquad (6.28)$$

As $I = 5/2$, a five-quantum experiment can be performed and has been indeed demonstrated experimentally.[42] Following the procedure cited above, the five-quantum coherence (corresponding to $(-5Q)$) is given by

$$\omega^{(2),static,5/2}_{-5/2,5/2} = \hbar^{-1}(E^{(2)}_{-5/2} - E^{(2)}_{5/2}) + 5\omega_{cs} \qquad (6.29)$$

Inserting the constant $C^{5/2}$ (eq 6.18), one obtains

$$\omega^{(2),static,5/2}_{-5/2,5/2} = C^{5/2}[-15/32\,\sin^2\beta_o(\sin^2\beta_o + 16\cos^2\beta_o)] + 5\omega_{cs} \qquad (6.30)$$

A geometrical representation is given by

$$-(15/32)(X^2+Y^2)[16Z^2+(X^2+Y^2)] = \pm 1 \qquad (6.31)$$

One of these surfaces is imaginary. Under rapid rotation, these equations become

$$A^{5/2}_{-5/2,+5/2}(X^2+Y^2)^2 + B^{5/2}_{-5/2,+5/2}Z^4 + C^{5/2}_{-5/2,+5/2}Z^2(X^2+Y^2) = \pm 1 \qquad (6.32)$$

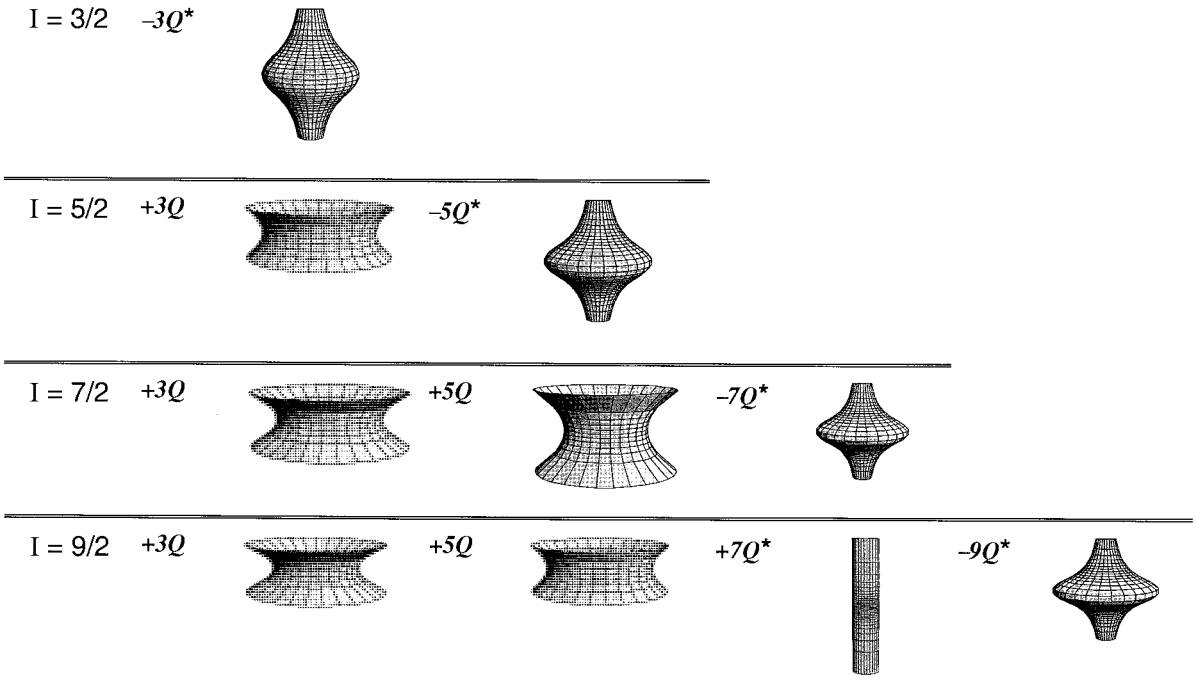

Figure 13. Representation in the PAS of the multiple-quantum coherences for every $I = n/2$ value ($n = 3, 5, 7, 9$). When possible, the + equation is used. *One of the corresponding surfaces is imaginary.

with

$$A^{5/2}_{-5/2,+5/2} = (3/256)(225\cos^4\beta - 170\cos^2\beta - 95)$$

$$B^{5/2}_{-5/2,+5/2} = (3/32)(75\cos^4\beta - 70\cos^2\beta - 5)$$

$$C^{5/2}_{-5/2,+5/2} = (3/32)(-225\cos^4\beta + 190\cos^2\beta - 45) \quad (6.33)$$

Transposing eqs 6.24, the condition for high resolution is obtained for

$$2(-175/64 + (21/16)t_e)\cos^3\beta + (75/32 - (9/8)t_e)\cos\beta = 0 \quad (6.34)$$

The echo occurs at $t_e = 25/12$. One obtains consequently

$$C^{5/2}\,C_6 = (40/9)\frac{\pi^2}{\omega_o}\left[\frac{3C_Q}{2I(2I-1)}\right]^2 = -(25/6)\omega^{(2),\mathrm{iso}}_{-1/2,1/2} \quad (6.35)$$

with $(\pm r_\beta{}^{-4})^{5/2}_{-5/2,+5/2} + t_e(\pm r_\beta{}^{-4})_{-1/2,1/2} = C_6$ (C_6 is a constant). The attained isotropic shift is then given by

$$\omega^{(2),\mathrm{iso},5/2}_{-5/2,5/2} = -(25/6)\omega^{(2),\mathrm{iso}}_{-1/2,1/2} + (85/12)\omega_{cs} \quad (6.36)$$

Our pictorial approach of the MQ-MAS experiment can be extended to every $I = n/2$ ($n = 3, 5, 7, 9$) spin and to every order of coherence. All needed parameters are presented in Table 3, including (i) the constant $C^{I=n/2}$, (ii) the expression of $\omega^{(2),\mathrm{static},I=n/2}_{\pm m/2,\mp m/2}$ for m $\in$ [3,n], (iii) the equations of the surfaces connected to $\omega^{(2),\mathrm{static},I=n/2}_{\pm m/2,\mp m/2}$, (iv) the coefficients $A^{I=n/2}_{\pm m/2,\mp m/2}$, $B^{I=n/2}_{\pm m/2,\mp m/2}$, $C^{I=n/2}_{\pm m/2,\mp m/2}$ related to the averaged surfaces under rapid rotation, (v) the derived time for echo t_e, and (vi) the attained isotropic shift $\omega^{(2),\mathrm{iso},I=n/2}_{\pm m/2,\mp m/2}$. The involved surfaces are presented in Figure 13. One particular feature is related to the ($+7Q$) transition for $I = 9/2$. Indeed, the equations of the static fourth-degree surfaces are given by

$$(21/16)(X^2 + Y^2)^2 = \pm 1 \quad (6.37)$$

One of these surfaces is imaginary. The other one has the shape of a cylinder of revolution (with the Z axis of the PAS as the axis of revolution) but corresponds actually to a fourth-degree surface.

As a conclusion, we have shown that the abstract notion of multiple-quantum coherence as well as the MQ-MAS experiment can be safely illustrated by fourth-degree surfaces. In particular, the isotropic shifts on the F1 dimension (F2 corresponds to the anisotropic dimension) were derived easily. It is interesting to note that the "static" energy levels (eqs 2.25) are just needed for our pictorial approach. Moreover, the representation can be extended to the MQ-VAS experiment,[43] which involves $\theta \neq \zeta_m$ (θ corresponds to the angle between the rotor axis and B_o). Such a representation uses mostly the coefficients $A^{I=n/2}_{\pm m/2,\mp m/2}$, $B^{I=n/2}_{\pm m/2,\mp m/2}$, $C^{I=n/2}_{\pm m/2,\mp m/2}$ given in Table 3. The cases $I = 5/2$ and I = 3/2 ($(+3Q)$ and $(-3Q)$ coherences, respectively) are treated as examples. For $\theta \neq \zeta_m$ and $I = 5/2$, eqs 6.9 give:

$$(\pm r_\beta{}^{-4})^{\theta}_{-1/2,1/2} = A(\boldsymbol{\beta})\sin^4\theta + B(\boldsymbol{\beta})\cos^4\theta + C(\boldsymbol{\beta})\sin^2\theta\cos^2\theta \quad (6.38a)$$

$$(\pm r_\beta{}^{-4})^{5/2,\theta}_{+3/2,-3/2} = A^{5/2}_{+3/2,-3/2}\sin^4\theta + B^{5/2}_{+3/2,-3/2}\cos^4\theta + C^{5/2}_{+3/2,-3/2}\sin^2\theta\cos^2\theta \quad (6.38b)$$

If high resolution is attained in one dimension, the following equation must be fulfilled:

$$(\pm r_\beta{}^{-4})^{5/2,\theta}_{+3/2,-3/2} + t_e(\pm r_\beta{}^{-4})^{\theta}_{-1/2,1/2} = C_7 \quad (6.39)$$

(C_7 being a constant). By using the derivation of eq 6.39, one obtains

$$(-420\cos^4\theta + 360\cos^2\theta - 36)t_e = -665\cos^4\theta + 570\cos^2\theta - 57 \quad (6.40a)$$

$$(540\cos^4\theta - 408\cos^2\theta + 28)t_e = 855\cos^4\theta - 630\cos^2\theta + 39 \quad (6.40b)$$

This system can be solved in terms of (t_e, θ) and one obtains ($t_e^{\zeta_m} = 19/12$, ζ_m) corresponding to the MQ-MAS experiment and ($t_e^{\theta_1=70.12°} = 15/8$, $\theta_1 = 70.12°$), ($t_e^{\theta_2=30.56°} = 15/8$, $\theta_2 = 30.56°$). One can note that θ_1 and θ_2 are roots of $P_4(\cos\theta)$.

The case $I = 3/2$ can be treated following the same procedure. The obtained system of equations is then

$$(-315\cos^4\theta + 270\cos^2\theta - 27)t_e = -245\cos^4\theta + 210\cos^2\theta - 21 \quad (6.41a)$$

$$(135\cos^4\theta - 102\cos^2\theta + 7)t_e = 105\cos^4\theta - 90\cos^2\theta + 9 \quad (6.41b)$$

The solutions of eqs 6.41 are ($t_e^{\zeta_m} = 7/9$, ζ_m) corresponding to the MQ-MAS experiment and ($t_e^{\theta_1=70.12°} = 0$, $\theta_1 = 70.12°$), ($t_e^{\theta_2=30.56°} = 0$, $\theta_2 = 30.56°$). For rapid rotation of samples at $\theta_{1,2}$, the echo occurs "immediatly" as $t_e^{\theta_{1,2}} = 0$. This characteristic feature was first noted by Amoureux[44] in the frame of the variable-angle spinning for three-half spins (VAST) methodology. However, overtone spectroscopy was involved in this particular case.

The VAST experiment can be illustrated in a different way. Indeed, for $\theta_1 = 70.12°$ or $\theta_2 = 30.56°$, the quantity

$$(\pm r_\beta^{-4})^{3/2,\theta_{1,2}}_{-3/2,3/2} = A^{3/2}_{-3/2,3/2}\sin^4\theta_{1,2} + B^{3/2}_{-3/2,3/2}\cos^4\theta_{1,2} + C^{3/2}_{-3/2,3/2}\sin^2\theta_{1,2}\cos^2\theta_{1,2}$$

is independent of β (this is shown by using eqs 4.18b and 6.8). In other words, high resolution is obtained for this transition under rapid rotation at θ_1 or θ_2.

Moreover, it can be noted that an MQ experiment involving θ_1 or θ_2 implies the total suppression of second-order broadening but allows the reintroduction of CSA and/or dipolar effects (as $\theta_{1,2} \neq \zeta_m$). Such experiments are interesting for the precise determination of coupled interactions and were recently implemented successfully.[43]

Let us consider an $I = 3/2$ nucleus, whose CSA parameters are ω_{11}, ω_{22}, and ω_{33} (principal components in angular velocity units). Moreover, we suppose that the CSA and quadrupolar PASs are coincident and $\omega_{ii} > 0$ ($i = 1, 2, 3$). Following the derivation of eqs 2.23 and 2.25, surfaces accounting for the second-order quadrupolar broadening and CSA under static conditions are obtained. For the (−1/2,1/2) central transition

$$(3/8)(X^2 + Y^2)[8Z^2 - (X^2 + Y^2)] = \pm 1 \quad (6.42a)$$

corresponds to the second-order quadrupolar broadening (see eq 2.19).

$$\omega_{11}X^4 + \omega_{22}Y^4 + \omega_{33}Z^4 + (\omega_{11} + \omega_{22})X^2Y^2 + (\omega_{11} + \omega_{33})X^2Z^2 + (\omega_{22} + \omega_{33})Y^2Z^2 = \pm 1 \quad (6.42b)$$

corresponds to CSA. For the triple-quantum coherence,

$$-(3/8)(X^2 + Y^2)[8Z^2 + (X^2 + Y^2)] = \pm 1 \quad (6.43a)$$

corresponds to the second-order quadrupolar broadening (see eqs 6.5−6.6).

$$3\{\omega_{11}X^4 + \omega_{22}Y^4 + \omega_{33}Z^4 + (\omega_{11} + \omega_{22})X^2Y^2 + (\omega_{11} + \omega_{33})X^2Z^2 + (\omega_{22} + \omega_{33})Y^2Z^2\} = \pm 1 \quad (6.43b)$$

corresponds to CSA. Under rapid rotation and using eqs 4.3−4.4 and 6.7−6.8, the corresponding averaged surfaces are derived. For the central transition,

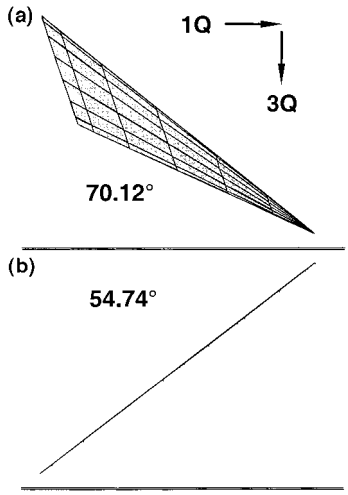

Figure 14. (a) Pictorial representation of the MQ-VAS experiment ($I = 3/2$, $\theta = 70.12°$). The obtained 2D maps correspond to a correlation between a 1Q and a 3Q dimensions. (b) When $\theta = 54.74°$, a straight line is obtained and corresponds to the MQ-MAS experiment (ref 43).

$$A(\boldsymbol{\beta})(X_R^2 + Y_R^2)^2 + B(\boldsymbol{\beta})Z_R^4 + C(\boldsymbol{\beta})Z_R^2(X_R^2 + Y_R^2) = \pm 1 \quad (6.44a)$$

$$N(\boldsymbol{\alpha},\boldsymbol{\beta})(X_R^2 + Y_R^2)^2 + O(\boldsymbol{\alpha},\boldsymbol{\beta})Z_R^4 + P(\boldsymbol{\alpha},\boldsymbol{\beta})Z_R^2(X_R^2 + Y_R^2) = \pm 1 \quad (6.44b)$$

with

$$N(\boldsymbol{\alpha},\boldsymbol{\beta}) = \frac{1}{2}\{-\cos^2\beta[\cos^2\alpha(\omega_{22} - \omega_{11}) + \omega_{33} - \omega_{22}] - \cos^2\alpha(\omega_{11} - \omega_{22}) + \omega_{11} + \omega_{33}\}$$

$$O(\boldsymbol{\alpha},\boldsymbol{\beta}) = \cos^2\beta[\cos^2\alpha(\omega_{22} - \omega_{11}) + \omega_{33} - \omega_{22}] + \cos^2\alpha(\omega_{11} - \omega_{22}) + \omega_{22}$$

$$P(\boldsymbol{\alpha},\boldsymbol{\beta}) = \frac{1}{2}\{\cos^2\beta\,[\cos^2\alpha\,(\omega_{22} - \omega_{11}) + \omega_{33} - \omega_{22}] + \cos^2\alpha\,(\omega_{11} - \omega_{22}) + \omega_{11} + 2\omega_{22} + \omega_{33}\} \quad (6.45)$$

For the triple-quantum coherence,

$$A^{3/2}_{-3/2,3/2}(X_R^2 + Y_R^2)^2 + B^{3/2}_{-3/2,3/2}Z_R^4 + C^{3/2}_{-3/2,3/2}Z_R^2(X_R^2 + Y_R^2) = \pm 1 \quad (6.46a)$$

$$3\{N(\boldsymbol{\alpha},\boldsymbol{\beta})(X_R^2 + Y_R^2)^2 + O(\boldsymbol{\alpha},\boldsymbol{\beta})Z_R^4 + P(\boldsymbol{\alpha},\boldsymbol{\beta})Z_R^2(X_R^2 + Y_R^2)\} = \pm 1 \quad (6.46b)$$

The MQ-VAS experiment can be understood as a 2D correlation between the central transition and the triple quantum coherence. Using eqs 6.45−6.46, $\{(\pm r_{\alpha,\beta}^{-4})^{3/2,\theta_{1,2}}_{-3/2,3/2}, (\pm r_{\alpha,\beta}^{-4})^{\theta_{1,2}}_{-1/2,1/2}\}$ corresponds to a point in a 2D map ($\theta_1 = 70.12°$, $\theta_2 = 30.56°$). Such a correlation map for $\theta_1 = 70.12°$ (in arbitrary units) is presented in Figure 14a and is analogous to those presented by Wang and co-workers.[43]

When $\theta = \zeta_m$ (Figure 14b), the map is particularly simple and corresponds to a straight line. In this case, the correlation

CHART 1

$$\mathbf{P} = \begin{bmatrix} a & d & g \\ b & e & h \\ c & f & i \end{bmatrix} = \begin{bmatrix} (\cos\alpha\cos\beta\cos\gamma - \sin\alpha\sin\gamma) & (-\cos\alpha\cos\beta\sin\gamma - \sin\alpha\cos\gamma) & (\cos\alpha\sin\beta) \\ (\sin\alpha\cos\beta\cos\gamma + \cos\alpha\sin\gamma) & (-\sin\alpha\cos\beta\sin\gamma + \cos\alpha\cos\gamma) & (\sin\alpha\sin\beta) \\ (-\sin\beta\cos\gamma) & (\sin\beta\sin\gamma) & (\cos\beta) \end{bmatrix}$$

experiment corresponds then to MQ-MAS: high resolution is attained in one dimension.

It can be further noted that CSA is represented by a fourth-degree expression (see eq 6.42b). Such an expression is used for the homogeneity with the second-order quadrupolar terms in the equations. Quadrics (second-degree surfaces) may be also used.[10]

As a conclusion, several MQ experiments at different macroscopic angles have been illustrated by fourth-order surfaces and their averaged surfaces. Again, it can be noted that the only prerequisite is the knowledge of eqs 2.5.

7. Conclusion

In this article, we have shown that fourth-degree surfaces are able to represent second-order broadening effects on lines in solid-state NMR. More generally, the shifts involving fourth-degree polynomials of the basic trigonometric functions can be interpreted in terms of fourth-degree surfaces. In that sense, this approach is an extension of the representation of first-order effects by quadrics (that is, second-degree surfaces). Special attention was paid to the description of static quadrupolar and "dipolar−quadrupolar" effects. Moreover, it has been shown that the reorientation of samples could be taken into account by using derived averaged fourth-degree surfaces. Most results concerning MAS, VAS, DAS, DAH, DOR, and MQ-MAS (VAS) were analytically derived, avoiding the use of $P_2(\cos\theta)$ and $P_4(\cos\theta)$ Legendre polynomials. Nethertheless, the link between our approach and $P_2(\cos\theta)$, $P_4(\cos\theta)$ was established. The next step will be the interpretation of these surfaces in terms of invariants, to simplify further our representation. Indeed, the trace of a given second-rank symmetrical tensor is an invariant when considering averaged quadrics.[10] Analytical equations of averaged quadrics are then derived very easily, almost without any calculation. Moreover, it is obvious that the surfaces described above are connected to the frequency domain (in hertz). Maybe, it could be possible to use these surfaces (after inversion as $Hz^{-1} \equiv s$) for the description of pulse effects in the time domain. Work is now in progress for such a representation.

Appendix

Expression of the matrix **P** relating two frames oriented by the Euler angles (α, β, γ) defined in Figure 1 is shown in Chart 1.

$$X^4 = (a\mathrm{X_R} + d\mathrm{Y_R} + g\mathrm{Z_R})^4$$

$$Y^4 = (b\mathrm{X_R} + e\mathrm{Y_R} + h\mathrm{Z_R})^4$$

$$Z^4 = (cX_\mathrm{R} + fY_\mathrm{R} + iZ_\mathrm{R})^4$$

$$X^2Y^2 = (a\mathrm{X_R} + d\mathrm{Y_R} + g\mathrm{Z_R})^2\,(b\mathrm{X_R} + e\mathrm{Y_R} + h\mathrm{Z_R})^2$$

$$X^2Z^2 = (aX_\mathrm{R} + dY_\mathrm{R} + gZ_\mathrm{R})^2\,(c\mathrm{X_R} + f\mathrm{Y_R} + i\mathrm{Z_R})^2$$

$$Y^2Z^2 = (bX_\mathrm{R} + eY_\mathrm{R} + hZ_\mathrm{R})^2\,(cX_\mathrm{R} + fY_\mathrm{R} + iZ_\mathrm{R})^2$$

$a-i$ coefficients are given above.

References and Notes

(1) Bloembergen, N.; Rowland, T. J. *Phys. Rev.* **1955**, *97*, 1679.
(2) Pake, G. E. *J. Chem. Phys.* **1948**, *16*, 327.
(3) Pound, R. V. *Phys. Rev.* **1950**, *79*, 685.
(4) Stauss, G. H. *J. Chem. Phys.* **1964**, *40*, 1988.
(5) Haeberlin, U. *High-Resolution NMR in Solids, Selective Averaging*; Academic Press: New York, 1976; Chapter 2.
(6) Mehring, M. *Principles of High-Resolution NMR in Solids*, 2nd ed.; Springer-Verlag: Berlin, 1983; Chapter 2.
(7) Nye, J. F. *Physical Properties of Crystals*, 2nd ed.; Clarendon Press: Oxford, 1989; Chapter 1.
(8) Meier, B. *Chimia* **1994**, *48*, 56.
(9) Radeglia, R. *Solid State NMR* **1995**, *4*, 317.
(10) Bonhomme, C.; Livage, J. *J. Phys. Chem. A* **1998**, *102*, 375.
(11) Abragam, A. *Principles of Nuclear Magnetism*; Clarendon Press: Oxford, 1989; Chapter 7.
(12) Andrew, E. R.; Bradbury, A.; Eades, R. G. *Nature* **1958**, *182*, 1659.
(13) Lowe, I. J. *Phys. Rev. Lett.* **1959**, *2*, 285.
(14) Samoson, A.; Kundla, E.; Lippmaa, E. *J. Magn. Reson.* **1982**, *49*, 350.
(15) Freude, D.; Haase, J. *NMR Basic Principles and Progress*; Springer-Verlag: Berlin, 1993; Vol. 29.
(16) Chmelka, B. F.; Zwanziger, J. W. *NMR Basic Principles and Progress*; Springer- Verlag: Berlin, 1994; Vol. 33.
(17) Llor, A.; Virlet, J. *Chem. Phys. Lett.* **1988**, *152*, 248.
(18) Chmelka, B. F.; Mueller, K. T.; Pines, A.; Stebbins, J.; Wu, Y.; Zwanziger, J. W. *Nature* **1989**, *339*, 42.
(19) Mueller, K. T.; Sun, B. Q.; Chingas, G. C.; Zwanziger, J. W.; Terao, T.; Pines, A. *J. Magn. Reson.* **1990**, *86*, 470.
(20) Samoson, A.; Lippmaa, E.; Pines, A. *Mol. Phys.* **1988**, *65*, 1013.
(21) Samoson, A.; Pines, A. *Rev. Sci. Instrum.* **1989**, *60*, 3239.
(22) Frydman, L.; Harwood, J. S. *J. Am. Chem. Soc.* **1995**, *117*, 5367.
(23) Medek, A.; Harwood, J. S.; Frydman, L. *J. Am. Chem. Soc.* **1995**, *117*, 12779.
(24) Harris, R. K. *Multinuclear Magnetic Resonance in Liquids and Solids—Chemical Applications*; Kluwer Academic: Dordrecht, 1990; Chapter 15.
(25) Man, P. P. *Encyclopedia of Nuclear Magnetic Resonance*; Wiley: Chichester, 1996; Vol. 6, p 3838.
(26) Olivieri, A. C.; Frydman, L.; Diaz, L. E. *J. Magn. Reson.* **1987**, *75*, 50.
(27) Naito, A.; Ganapathy, S.; McDowell, C. A. *J. Chem. Phys.* **1981**, *74*, 5393.
(28) Harris, R. K.; Jonsen, P.; Packer, K. J. *Magn. Reson. Chem.* **1985**, *23*, 565.
(29) Opella, S. J.; Frey, M. H.; Cross, T. A. *J. Am. Chem. Soc.* **1979**, *101*, 5856.
(30) Schramm, S.; Oldfield, E. *J. Am. Chem. Soc.* **1984**, *106*, 2502.
(31) Ganapathy, S.; Schramm, S.; Oldfield, E. *J. Chem. Phys.* **1982**, *77*, 4360.
(32) Ramakrishna, J.; Ajoy, G. *Solid State NMR* **1995**, *4*, 125.
(33) Lefebvre, F.; Amoureux, J. P.; Fernandez, C.; Derouane, E. G. *J. Chem. Phys.* **1987**, *86*, 6070.
(34) Samoson, A.; Sun, B. Q.; Pines, A. *Pulsed Magnetic Resonance: NMR, ESR and Optics*; Clarendon Press: Oxford, 1992; Chapter 3.
(35) Wooten, E. W.; Mueller, K. T.; Pines, A. *Acc. Chem. Res.* **1992**, *25*, 209.
(36) Sun, B. Q.; Baltisberger, J. H.; Wu, Y.; Samoson, A.; Pines, A. *Solid Sate NMR* **1992**, *1*, 267.
(37) Gann, S. L.; Baltisberger, J. H.; Pines, A. *Chem. Phys. Lett.* **1993**, *210*, 405.
(38) Bax, A.; Szeverenyi, N. M.; Maciel, G. E. *J. Magn. Reson.* **1983**, *52*, 147.
(39) Amoureux, J. P. *Solid State NMR* **1995**, *4*, 229.
(40) (a) Massiot, D.; Touzo, B.; Trumeau, D.; Coutures, J. P.; Virlet, J.; Florian, P.; Grandinetti, P. J. *Solid State NMR* **1996**, *6*, 73. (b) Wu, G.; Rovnyak; D.; Huang, P. C.; Griffin, R. G. *Chem. Phys. Lett.* **1997**, *277*, 79. (c) Wu, G.; Rovnyak, D.; Griffin, R. G. *J. Am. Chem. Soc.* **1996**, *118*, 9326. (d) Dirken, P. J.; Kohn, S. C.; Smith, M. E.; van Eck, E. R. H. *Chem. Phys. Lett.* **1997**, *266*, 568. (e) Massiot, D. *J. Magn. Reson. A* **1996**, *122*, 240. (f) Wu, G.; Rovnyak, D.; Sun, B. Q.; Griffin, R. G. *Chem. Phys. Lett.* **1996**, *249*, 210. (g) Amoureux, J. P.; Fernandez, C.; Frydman, L. *Chem. Phys. Lett.* **1996**, *259*, 347. (h) Hanaya M.; Harris, R. K. *Solid State NMR* **1997**, *8*, 147. (i) Wu, G.; Kroeker, S.; Wasylishen, R. E.; Griffin, R. G. *J.*

Magn. Reson. **1997**, *124*, 237. (j) Duer, M. J.; Strourton, C. *J. Magn. Reson*. **1997**, *124*, 189. (k) Brown, S. P.; Wimperis, S. *J. Magn. Reson*. **1997**, *124*, 279. (l) Hanaya, M.; Harris, R. K. *J. Phys. Chem. A* **1997**, *101*, 6903. (m) Duer, M. J. *Chem. Phys. Lett*. **1997**, *277*, 167. This list is not exhaustive.

(41) Man, P. P. *Phys. Rev. B* **1997**, *55*, 8406.

(42) Fernandez, C.; Amoureux, J. P.; Chezeau, J. M.; Delmotte, L.; Kessler, H. *Microporous Mater*. **1996**, *6*, 331.

(43) Wang, S. H.; Xu, Z.; Baltisberger, J. H.; Bull, L. M.; Stebbins, J. F.; Pines, A. *Solid State NMR* **1997**, *8*, 1.

(44) Amoureux, J. P. *Solid State NMR* **1993**, *2*, 83.